Spring 2015

Characterization of the *C. elegans* nascent polypeptide associated complex (NAC) function under stress

Jonathan E. Sandoval
James Madison University

Characterization of the *C. elegans* nascent polypeptide associated complex (NAC) function under stress

Jonathan Sandoval

A thesis submitted to the Graduate Faculty of

JAMES MADISON UNIVERSITY

In

Partial Fulfillment of the Requirements

for the degree of

Master of Science

Department of Biology

May 2015

Contents

List of figures

Abstract

The nascent polypeptide-associated complex (NAC) is a highly conserved heterodimer known to play an important role in protein folding and localization during metazoan development. Evidence in different model systems indicates that removal of either subunit of the NAC, i.e. α- or β-NAC, is sufficient to generate misfolded protein stress in the endoplasmic reticulum (ER), resulting in the activation of the ER-specific unfolded protein response (UPR). What is not yet understood is the nature of the UPR depending on which subunit of the NAC is depleted. My research is focused on characterizing the specific UPR outcomes induced upon depletion of either α- or β-NAC during misfolded protein stress in the ER. Assessment of UPR outcomes revealed that depletion of the *C. elegans* NAC homologues *icd-1/*□NAC and *icd-2/*□NAC shared unique responses relative to the subunit depleted. Specifically, depletion of ICD-1 led to increased ER specific chaperone expression and robust attenuation of protein synthesis when compared to depletion of ICD-2. Along with managing protein homeostasis during ER stress, I also found that specific components of the NAC and UPR actively contribute to cell differentiation programs, e.g. embryos depleted of ICD-1 displayed altered neuronal marker expression during ER stress, while other cell-type specific markers remained unchanged. These results suggest the individual subunits of the *C. elegans* NAC are functional when unbound and contribute differentially to the activation of the UPR when one subunit is in excess relative to the other. Such findings may provide insights into the pathology of diseases such as Alzheimer's, in which the 1:1 stoichiometry of the NAC subunits is disrupted.

1 Introduction

1.1 Protein folding

Cells require functional proteins to survive and reproduce. To achieve a functional native state, proteins must first properly fold. Prior to attaining a terminally functional conformation, nascent polypeptides traverse various unfavorable conformations that, if retained, would result in misfolded non-functional proteins or misfolded proteins possessing altered functionality[1, 2]. Given the importance of achieving accurately folded proteins for cell viability, how do cells respond in the presence of increased levels of misfolded proteins? One coping mechanism is induction of protein degradation processes such as the ubiquitin proteasome system, which degrades misfolded proteins tagged with multiple ubiquitins. However, because protein synthesis is energetically costly, engaging protein degradation mechanisms may be a wasteful expenditure of energy if not necessary. On the other hand, failure to remove misfolded proteins may have detrimental effects on cellular function. Therefore in an attempt to avoid the degradation of energetically costly proteins without compromising cellular integrity, cells employ various quality-control mechanisms to ensure accurately folded mature polypeptides[3, 4].

A critical mechanism employed for proper protein folding is the induction of chaperones. This system assists protein folding by preventing incompletely folded polypeptide chains from forming unfavorable interactions while also lowering the activation energy of energetically unfavorable folding steps that polypeptide chains often have to traverse to achieve their final structure[5]. Due to the complex and highly congested environment in which proteins must reach their native state, proper folding

often requires auxiliary folding mechanisms (e.g. chaperones)[6, 7]. However, under appropriate in vitro conditions proteins are able to reach a native functional conformation in the absence of chaperones[8]. This evidence suggests polypeptide chains hold sufficient instructions to direct their own folding, but additional support systems are required due to the complex cellular environment in which the protein is folding. To fully understand the process of protein folding, one needs to understand the numerous elements integral to this process, how they function to drive proper folding and how the cell responds when these systems falter.

Protein folding is an extensively regulated process essential for cellular function and viability. Alterations to this process often have adverse effects. Under circumstances typically involving exogenous stressors, proteins may fail to fold properly during translation or, once folded, retain their native state. This failure is often sufficient to trigger stress-response mechanisms that can initiate the death of the cell via apoptosis[9]. Apoptosis is a genetically well-defined mechanism that triggers the activation of caspases and proteases that cleave specific cellular targets to result in the death of the cell. Apoptosis removes damaged cells that could otherwise be dangerous to the organism such as cells containing a large number of misfolded proteins[10]. As such, diseases that generate misfolded protein stress affect the initiation of apoptosis; most neurodegenerative disorders generate large numbers of misfolded proteins that result in neuronal apoptosis, while a vast majority of cancers up-regulate protein-folding mechanisms during rapid cell division to avoid misfolded protein stress and the initiation of apoptosis[11, 12]. The direct link between misfolded protein stress and disease

necessitates a clear understanding of protein folding mechanisms, how they function in healthy cells, and how they malfunction during disease pathology.

Neurodegenerative diseases such as Alzheimer's disease (AD), Parkinson's disease (PD), Huntington's disease (HD), amyotrophic lateral sclerosis (ALS) and prion diseases share a common pathogenic mechanism while possessing diverse genetic predispositions. A reoccurring theme in neurodegenerative diseases is the formation of insoluble fibrils resulting from misfolded protein aggregates[11]. Alterations in protein homeostasis, sequentially leading to misfolded proteins, produce these aggregates which mainly consist of repeating fibers composed of misfolded proteins in a β-sheet conformation[11, 13]. These insoluble fibrils are responsible for the neuronal apoptosis that produces the phenotypes commonly observed in neurodegenerative diseases, e.g. loss of motor control and decreased cognitive function[17]. It is therefore evident that apoptosis, triggered by the presence of intractable misfolded proteins, is a fundamental process of disease onset and progression[14].

In healthy cells, mechanisms that control the quality of protein folding bind nascent polypeptide chains during translation and prevent the formation of inappropriate tertiary structures to yield a mature functional protein[15, 16]. However, quality control mechanisms appear to malfunction during neurodegeneration, that is, proteins in neurons fail to reach a native conformation, resulting in pre-mature apoptosis in these cells[17]. This outcome is likely due to a decreased or desensitized ability to cope with increased misfolded proteins, a theory supported by the decreased chaperone activity commonly observed in neurodegenerative disease[18]. Cells undergoing stress must critically engage folding mechanisms to adapt and prevent lethal levels of proteotoxicity[19]. That cells are

able to withstand certain levels of misfolded protein stress and remain viable reveals the existence of a response that mitigates this stress and triggers apoptosis only when a threshold is exceeded. As such, one plausible contribution to neurodegeneration is when upstream regulatory factors fail to properly activate compensatory folding mechanisms, triggering cell death well below levels that would normally trigger cell death.

As with neurodegeneration, cancer is another class of disease intimately associated with protein folding and apoptosis, but in a much different way. Pre-cancerous as well as cancerous cells often proliferate at an above average rate, requiring the accelerated expression of certain proteins that are often unable to fold properly and are, therefore, abnormal in function[20]. Normally, this scenario would lead to the rapid accumulation of misfolded protein and eventually apoptosis; such a response by stress response mechanisms that initiate apoptosis protects the organism. How do successful cancerous cells mitigate, or even prevent, the increased misfolded protein stress that can lead to apoptosis? The "micro-evolution" of a cancer cell provides an answer [21]. Pre-cancerous cells unable to withstand the pressure of sustained levels of misfolded proteins stress will eventually undergo apoptosis and die[12]. Successful cancer cells survive this pressure and evade apoptosis due to the acquisition of mutations that allow the cell to manage the dramatically increased rates of protein synthesis, both functional and misfolded, during rapid cell divisions. Due to the increased proliferation of most tumor cells, in combination with mutations that often affect protein structure, proteins in these cells, on average, possess less than one quarter the half-life when compared to proteins in healthy cells[22]. This increase in protein turnover is accompanied by increased translation and protein-folding capacity in the form of elevated chaperone expression. As proteins of

the highly mutable cancerous cells become unstable, chaperone activity increases[23]. Consistently, the vast majority of tumors, regardless of type, overexpress heat shock proteins, including of those in the HSP90 and -70 families[12]. In addition, successful cancerous cells are thought to contain other mechanisms for coping with increased misfolded protein stress, including those that regulate chaperone activity. As with neurodegeneration, understanding the role of protein folding and misfolded protein stress-response in cancer development will likely provide insights into disease pathology and treatment.

1.2 The Unfolded Protein Response (UPR) and its role in misfolded protein stress

The establishment and maintenance of proper protein folding and turnover, otherwise known as protein homeostasis, is essential for maintaining cellular integrity, and cells possess robust and redundant systems dedicated to this process. In eukaryotes, the endoplasmic reticulum (ER) is essential for the folding and modification of both secreted and transmembrane proteins. The protein folding process in the ER involves several steps, increasing the possibility that any individual step may generate a misfolded protein. As a buffer against the accumulation of misfolded protein, the ER contains a network of mechanisms that can mitigate potential proteotoxic levels of misfolded proteins within the organelle [24, 25, 26]. This network of stress responses is collectively known as the unfolded protein response, or UPR.

The UPR is an ER-specific misfolded protein sensor that determines the fate of a cell under misfolded protein stress. Highly conserved amongst eukaryotic organisms, the UPR is activated in response to misfolded protein accumulation in the ER and maintains homeostasis through several mechanisms that mitigate the accumulation of misfolded

protein, including: 1) increased expression of ER-specific chaperones; 2) attenuation of protein synthesis, and; 3) translocation of terminally misfolded proteins from the ER to the cytosol for proteosomal degradation[27]. These interventions can rescue cells undergoing low levels of misfolded protein stress for relatively short periods of time. However, under acute and/or sustained levels of misfolded protein stress, the UPR is often unable to adequately suppress the accumulation of misfolded protein, and a proteotoxic environment ensues. In these cases the UPR typically triggers cell death, primarily via apoptosis[27]. As such, the components of the UPR cooperate to control the balance between cell survival and cell death in the face of misfolded protein stress, a balance determined by the length and intensity of the stress.

The UPR consists of three ER transmembrane proteins that work in parallel to engage various signal transduction pathways. Inositol-requiring enzyme-1 (IRE1), protein kinase RNA-like endoplasmic reticulum kinase (PERK) and activating transcription factor-6 (ATF6) each have the ability to sense misfolded protein stress in the ER and initiate responses to manage the resulting stress[27]. While a number of responses are generated by the UPR, three specific outcomes appear to be essential to save the cell: attenuation of translation, up-regulation of chaperone expression and degradation of misfolded protein. Each outcome results directly from UPR activity, and in some cases these signaling pathways behave redundantly[27].

The three arms of the UPR are maintained in an inactive state in the absence of misfolded protein stress in the ER, primarily through an interaction with glucose-regulated protein-78 (GRP78)/BiP, a highly conserved ER-specific chaperone that controls the activation of UPR signaling[28]. GRP78/BiP binds to the lumenal moiety of

each component, preventing activation; this chaperone possesses a higher affinity, though, for misfolded proteins. Increases in levels of misfolded proteins titrate GRP78/BiP away from IRE1, PERK and ATF6, allowing for their activation[29]. As such, GRP78/BiP behaves as a sensor of misfolded protein stress in the ER that modulates response; as more misfolded protein accumulates, more GRP78/BiP dissociates from UPR components, strengthening the stress response in parallel with the accumulation of misfolded protein.

One can understand the complete contribution of the UPR to management of misfolded protein stress by analyzing the individual contributions made during this response, including the attenuation of translation. Provided with the appropriate stimuli, PERK dissociates from GRP78/BiP and homodimerizes to promote its auto phosphorylation and activation. PERK subsequently phosphorylates the α-subunit of eukaryotic initiation factor-2 (eIF2α), preventing the formation of the eIF2α-tRNAmet-40S translation initiation complex[30, 31]. Phosphorylation of eIF2α represses general translation, but paradoxically promotes the translation of the pro-survival activating transcription factor-4 (ATF4) and the pro-apoptotic factor C/EBP homologous protein (CHOP) [32]. In this way, PERK activation and the resulting attenuation of translation ultimately leads to the generation of both pro-survival and pro-apoptotic signals. An additional outcome of Phosphorylated eIF2α is ATF4 dependent expression of ER stress response element (ERSE) target genes[33]. The ERSE promoter domain targets the expression of specific genes containing this conserved motif, such as ER specific chaperones GRP78/BiP and GRP94, in the presence of ER stress[34]. ATF6 and IRE1

contribute to transcriptional up-regulation of ER-specific chaperones thus activation of ERSE target genes reflects the overlap amongst components of the UPR[35, 36, 37].

The increased expression of ATF4 leads to the up regulation of chaperone production via the transcription factor's ability to bind to the ER stress response element (ERSE). In fact, all three arms of the UPR are able to increase chaperone expression via the ERSE. During the UPR, activated ATF6 migrates from the ER to the Golgi apparatus where the protein is cleaved to reveal its nuclear localization domain and subsequently acts as a transcription factor to directly up regulate the expression of ER specific chaperones responsible for augmenting ER folding capacity[35, 36]. In addition, IRE1 indirectly induces the transcription of ERSE target genes using intrinsic endoribonuclease activity to splice a 26 base intron from the mRNA of the X-box binding protein-1 (XBP1) transcription factor. The subsequent translation of this mRNA generates a potent transcription factor that induces ER specific chaperone expression via ERSE. Depending on the source and strength of the misfolded protein stress in the ER, one or more of these arms of the UPR can lead to a dramatic increase in chaperone expression, contributing to the mitigation of the stress and the rescue of the cell[37].

In addition to the attenuation of translation and increase in expression of chaperones, successful rescue of stressed cells requires the degradation of proteins misfolded beyond repair. To prevent accumulation of these proteins in the ER, the UPR induces their retro-translocation to the cytosol for degradation primarily via the ubiquitin proteasome system in a process termed ER-associated degradation (ERAD). During this process, E1, E2 and E3 ubiquitin ligases covalently link ubiquitin to misfolded proteins. Carrier proteins containing an Ubl or Uba structural domains bring tagged proteins to the

proteosome for enzymatic degradation and recycling of the resulting amino acids[38]. Autophagy-mediated ERAD involves the formation of small double membrane structures termed autophagosomes. Autophagsomes collect dysfunctional organelles as well as misfolded proteins and fuse with lysosomes, leading to the breakdown of materials within these structures primarily by proteases[39]. The UPR triggers the initiation of ERAD by facilitating the conversion of LC3, a pro-autophagic regulator essential for the formation of autophagosomes. LC3 conversion requires pro-LC3 cleavage to yield LC3-I in the cytosol. Cleaved LC3-I is further modified with the addition of phospholipids to LC3-II, which forms the membrane structure of autophagosomes[40]. PERK activity, leading to eIF2α phosphorylation, indirectly contributes to autophagy-mediated ERAD via direct eIF2α up regulation of LC3[41].

The intended outcome of the UPR-initiated events detailed above is to "buy" the cell time to mitigate the level of misfolded protein and survive. If misfolded proteins continue to accumulate regardless of the cell-saving pathways employed, the UPR has the ability to initiate apoptosis, thereby eliminating a cell in which the damage is beyond rescue[42]. Apoptosis can be initiated via the PERK or IRE1 pathway, but in either case, the loss of the cell is double-edged sword; elimination of damaged cells can prevent further damage to healthy cells to help maintain organismal viability, but depending on the cell type eliminated, this cell death can also leave the organism debilitated, negatively affecting viability. To understand how misfolded protein stress is well-managed in healthy cells, and perhaps mismanaged during disease, my research is focused on what appears to be a central component to this process, a translational chaperone known as the nascent polypeptide-associated complex, or NAC.

1.3 The NAC and its contributions to the management of misfolded protein stress

As a translational chaperone responsible for assisting in both protein transport and folding during translation, the nascent polypeptide associated complex (NAC) is an integral component of protein homeostasis. The NAC is a heterodimeric complex composed of a α- and β- subunit bound to the ribosome near the polypeptide exit tunnel. Like other co-translational chaperones, the NAC is thought to associate with nascent polypeptide chains exiting the ribosome to ensure proper folding and transport. In addition, the NAC appears to contribute to stress responses regulated by the UPR[43]. Due to the overlapping functions between the NAC and the UPR in regulating protein homeostasis, the NAC is a suitable candidate for exploring misfolded protein stress coping mechanisms in relation to the UPR.

For the NAC to engage its function as a ribosomal co-translational chaperone, the α- and β- subunits must be in a 1:1 stoichiometry[44]. Although to date the molecular function of the NAC has not been precisely defined, the heterodimeric complex appears to have numerous roles and has been implicated as a 1) transcription regulator, 2) translation regulator, 3) ribosomal chaperone, 4) ER trans-locater, 5) mitochondrial trans-locater, 6) negative regulator of apoptosis and 7) regulator of autophagy[45, 46]. Studies involving the yeast NAC homolog, composed of Edg1 (β- subunit) and Edg2 (α-subunit), suggest that the NAC functional complex is a translational chaperone that interacts with cytosolic chaperones[47, 48, and 49]. This is based on evidence showing the N-terminus of Egd1 binds the ribosome close to the amino acid exit tunnel as well as specifically binding to the ribosomal protein rpl-31[50, 51]. Pech et al. also showed Edg2 can bind to ribosomal protein rpl-17, a protein neighboring rpl-31. Both rpl-31 and rpl-

17 are surrounded by rRNA and in close proximity with newly folding peptides as they exit the ribosome[51]. The crystal structure of human α-NAC revealed a nucleic-acid binding region within the α-subunit that possesses a stronger affinity for ssRNA than DNA, suggesting the NAC may stabilize binding of the ribosomal complex via an association with rRNA surrounding the amino-acid exit site[52, 53]. Furthermore, rpl-31 is a contact point for the co-chaperone ribosome associated complex (RAC) and the ER translocation signal recognition particle (SRP) protein receptor[54, 55]. Double deletions of the RAC chaperone partner stress 70 B (SSB) and the NAC led to synergistic growth defects and increased sensitivity to translation inhibitors[56]. In addition, yeast NAC associates with nearly all nascent peptides on translating ribosomes and modulates SRP binding to nascent peptides[49]. In combination, these observations support the hypothesis that the NAC is a translational chaperone that regulates SRP receptor binding to the ribosome therein affecting translocation of proteins into the ER.

While the NAC function appears to be essential for proper protein folding and localization in healthy cells, its individual subunits also appear to contribute protective functions in cells undergoing misfolded protein stress. During sustained stress, βNAC is thought to both dissociate from ribosomes and function as a cytosolic chaperone to prevent protein aggregation. βNAC is able to interact with the major cytosolic chaperone family members HSP70 and HSP90 while lacking the canonical ATPase domain found in most chaperones[57]. Therefore βNAC likely acts as a cytosolic chaperone in a cooperative manner to maintain proteostasis. In addition to βNAC's independent function, the α-NAC subunit possesses a nucleic acid binding region that is exposed only after dissociation from βNAC, allowing αNAC to function independently as a transcriptional

co-activator that may up regulate expression of GRP78/BiP[58]. With its varied roles as a complex and as individual subunits, the NAC is uniquely positioned to manage protein folding in both healthy cells and those undergoing misfolded protein stress[57]. However, these collective functions are likely engaged to varying extents based on stress severity as well as the cellular concentrations of individual NAC subunits.

Deletion of NAC-encoding genes in yeast generates no detectable defects, while NAC knockout mutations in higher eukaryotes, including fruit flies, worms and mice, lead to early embryonic arrest[59, 60, 61]. Therefore the lethal NAC mutant phenotype reflects the putative necessity of a functional complex and individual subunits for normal cell function, management of misfolded protein stress and overall viability.

βNAC depletion in *Caenorhabditis elegans* is sufficient to initiate ER stress and trigger up-regulation of ER-specific chaperones associated with the UPR[62]. Similarly, αNAC ablation by RNA interference in HeLa S3 cells leads to increased expression of several markers associated with an active UPR[63]. α- and βNAC have been implicated independently as negative regulators of the mitochondrial apoptotic pathway; consistent with the depletion of α or βNAC dramatically increasing apoptosis in cell cultures and *C. elegans* during embryogenesis, respectively[63, 64, 65]. Alternatively, α or βNAC over-expression is sufficient to rescue cells normally targeted to undergo apoptosis[64, 63]. It is important to note that in all of these experiments the levels of a single NAC subunit were altered (either α or βNAC) while the level of the remaining subunit remained unaltered. Together these results suggest a connection between the NAC, the UPR and the control of apoptosis during misfolded protein stress. As such, regulating the cellular concentration of NAC subunits relative to each other may serve as a way to cope with

misfolded protein stress and determine cell fate. Consistent with this model, NAC levels are altered in diseases associated with protein folding dynamics: βNAC is down-regulated in Alzheimer's disease, while αNAC is up-regulated in certain types of cancers[66, 67]. The potential involvement of NAC function in the pathology of human diseases emphasizes its importance, our need to understand its function and suggests independent functions of the individual NAC subunits likely arise upon activation of the UPR.

1.4 The role of α-NAC and the UPR in cellular differentiation

In addition to assisting cells in maintaining protein homeostasis under stress, alterations to cellular concentrations of αNAC appears to affect the normal progression of specific cell types through differentiation. During erythroid cell differentiation, αNAC is expressed in undifferentiated progenitor cells and is suppressed once progenitor cells become terminally committed. Ectopic αNAC expression in erythroid progenitor cells in culture leads to accelerated differentiation, whereas αNAC depletion in these same cells abolishes hemoglobin production[68]. In developing CD8+ T cells, αNAC expression is down regulated as differentiation progresses. Furthermore, αNAC ablation via antisense technology in human CD8+ T cells leads to increased levels of differentiation and of activation markers as well as increased cell proliferation[69]. Interestingly, during normal bone development osteoblasts express higher levels of αNAC mRNA relative to βNAC[70]. Phosphorylation of serine residue 43 translocates αNAC to osteoblast nuclei where it acts as a developmentally regulated transcriptional co-activator to increase bone matrix production. Knock-in mutant mice (αNAC-S43A) displayed decreased levels of nuclear

αNAC, inappropriate bone specific gene expression, decreased levels of immature bone tissues and increased levels of osteocyte differentiation markers[70].

The interaction of αNAC with the UPR is consistent with recent evidence implicating the UPR in the differentiation of specific cell types. αNAC transcriptional co-activator activity appears to regulate ATF4 mediated transcription during osteoblast development[71]. Similarly, α-NAC activity in erythroid cell differentiation parallels the strong activation of PERK in immature erythroid progenitor cells; both activities diminish as cells reach maturity[72]. In mice, experiments with hematopoietic cells carrying a fluorescent UPR reporter construct, that indicate IRE1-mediated XBP1 splicing is active during early stages of $CD8^+$ T cell differentiation and undetectable in a more mature $CD8^+$ T cell population, while IRE1 homozygous mutant mouse embryonic fibroblasts are defective in osteoblast differentiation[73]. Furthermore, the promoter region of the *osterix* transcription factor, an essential transcription factor for bone development, possesses two regulatory motifs that are bound by XBP1 during osteoblast development[74]. These observations support the notion that along with promoting protein homeostasis during ER stress, specific components of the NAC and UPR actively contribute to differentiation.

1.5 Experimental analysis and predictions

Our understanding of the role of the NAC in metazoans comes primarily from studies of the genetic model organism *C. elegans*, a ubiquitous nematode that has been widely used to elucidate the mechanisms of cell stress responses and apoptosis. In this regard, this organism has highly conserved pathways for both the UPR and apoptosis, and much of what we know about both processes was originally discerned in this organism.

C. elegans contains homologs of each of the three ER specific transmembrane proteins that constitute the UPR, and each pathway has been extensively studied in the context of knockout mutants[64, 75]. In addition, *C. elegans* is very well characterized for apoptosis, and its core apoptotic proteins are well conserved within a wide spectrum of species. As such, *C. elegans* provides the ideal model organism for the study of the NAC in relation to the UPR and apoptosis, as many of the extant mutants used to characterize the UPR and apoptosis provide an excellent starting point for elucidating the relationship of UPR stress response elements and the NAC.

Like its homologs, the *C. elegans* NAC consists of two subunits: ICD-1/β-NAC and ICD-2/α-NAC, both of which are required for viability. The nomenclature of these proteins, inhibitor of cell death (ICD), reflects the initial phenotype associated with the NAC in *C. elegans*; depletion of either subunit dramatically increases apoptosis during embryonic development, while overexpression of β-NAC suppresses apoptosis[64]. In subsequent studies, depletion of the NAC was also shown to induce misfolded protein stress in the ER, resulting in the up-regulation of the UPR[62]. While these findings have shed light on the relationship between the NAC, misfolded protein stress and cell death, many questions remain. Is the apoptosis observed upon depletion of either NAC subunit the direct result of UPR activity? Does depletion of one subunit of the NAC free the other subunit to function independently when the UPR is active? If so, do the dynamics amongst individual subunits of the NAC and the UPR lead to altered differentiation? Answers to these questions will provide insights into the role of the NAC in protein homeostasis and control of apoptosis during stress, and clarify how misregulation of the NAC might contribute to development of disease.

To test the hypothesis that the individual subunits of the NAC can function independently when the ER-specific UPR is active in *C. elegans*, a series of experiments were designed where *icd-1* and *icd-2* were removed by RNAi feeding in samples with an active UPR. RNAi depletion of either *icd*-1 or *icd-2* renders the other subunit in relative excess. This depletion strategy allowed for assessment of individual subunit activity in cells with an active UPR. Along with adult viability in these treatments and differences in differentiation, UPR specific outcomes were assessed: 1) ER specific chaperone expression and localization 2) changes in presence of lysosomes as a measure of increased protein degradation and 3) translation attenuation.

2 Methods

2.1 Maintenance of *C. elegans* stock strains

C. elegans strains were maintained at standard laboratory conditions on Carolina Nematode Growth Media (NGM) seeded with OP50 feeder bacteria. The OP50 feeder bacteria were generated from frozen stocks maintained at – 70° C that were shaken overnight in liquid LB broth at 37° C. Gravid adults were transferred to fresh NGM plates seeded with OP50 feeder every 3 to 5 days to maintain stock strains.

2.2 Mounting *C. elegans* embryos for microscope imaging

C. elegans embryos were mounted onto agar pads composed of 0.05 g Bacto agar per mL of dH_2O. To prevent sample desiccation during imaging, 10 µL of simple M9 buffer was evenly distributed throughout the agar pad. The simple M9 buffer was generated by mixing 3 g of KH_2PO_4, 11.3 g of $Na_2HPO_4 \bullet 7H_2O$, 5 g of NaCl and 1 mL of 1 M $MgSO_4$ to a final volume of 1 L dH_2O. The M9 buffer was autoclaved and allowed to cool at room temperature.

2.3 RNAi mediated depletion of proteins

RNA interference leads to depletion of protein levels by employing a genetically modified feeder bacteria that expresses a double-stranded RNA (dsRNA). The dsRNA is complementary to and targets the mRNA of the gene of interest for degradation. The feeder bacteria possess an engineered plasmid containing the dsRNA specific to the gene of interest under the control of an IPTG promoter. To generate engineered feeder bacteria, single colonies obtained from frozen stocks maintained at -70° C were suspended and shaken in liquid LB broth overnight at 37 C. To minimize contamination in the overnight engineered feeder bacteria culture, ampicillin was added to a final

concentration of 50 µg/mL of liquid LB broth. 250 µL of cultured feeder was seeded to RNAi plates. The RNAi plates were prepared by combining 4.5 g NaCl, 25.5 g agar, 3.75 g peptone, 1.5 mL of 2 mg/mL uracil, 0.22 g $CaCl_2$, and 0.75 ml of 10 mg/mL cholesterol in 1463 mL of dH_2O. After mixture was autoclaved and allowed to cool, 37.5 mL of phosphate buffer (pH 6), 1.5 mL of 1 M $MgSO_4$, 1.5 mL of 1 M IPTG, 1.5 mL 25 mg/mL carbenicillin and 0.3 mL of 50 mg/mL ampicillin was added. Seeded RNAi plates were dried at standard laboratory conditions for 24 hours. Upon assessment of various RNAi exposure times (24, 48 and 72 hours), 48 hour exposure yielded optimal depletion without proving fatal to the animal (data not shown). Therefore worms of similar age were placed on seeded RNAi plates for 48 hours for all RNA interference experiments.

2.4 tunicamycin induced ER stress

Tunicamycin is an antibiotic that leads to ER stress by inhibiting N-linked glycosylation in the ER, which leads to protein misfolding events. Studies across many organisms show tunicamycin exposure is sufficient to trigger the ER specific UPR[76]. To induce a UPR in adult nematodes and study embryonic effects, gravid worms were exposed to tunicamycin isolated from *Streptomyces lysosuperficus* (Calibiochem) subsequent to 48 hour RNAi depletion. 10 mg of tunicamycin was dissolved in 1 mL of DMSO and stored at -70 C. Tunicamycin plates were made by diluting the antibiotic to a final concentration of 5 µg/mL of NGM. Plates were seeded with OP50 feeder bacteria and allowed to dry in standard laboratory conditions for 24 hours. Preliminary data showed 48 hour tunicamycin exposure was optimal for assessing tunicamycin induced UPR. Therefore worms were first exposed to 48 hour RNAi depletion and then moved and maintained in the tunicamycin plates for 48 hours.

2.5 Monitoring viability in ICD-1, ICD-2 and UNC-22 depleted adult worms under tunicamycin

Three separate viability experiments were performed in worms containing an HSP-4::GFP fusion protein (Caenorhabditis Genetics Center University of Minnesota SJ4005). Viability was assessed in 30 gravid worms placed in tunicamycin plates subsequent to ICD-1, ICD-2 and a control UNC-22 depletion. Worms were maintained in tunicamycin plates for 48 hours at standard laboratory conditions and viable worms were counted every 12 hours throughout the duration of the experiment. Worms were prodded for movement with a heated platinum pick and samples displaying pharyngeal pumping as well as mobility were considered viable.

2.6 Monitoring HSP-4 expression in ICD-1, ICD-2 and UNC-22 depleted live embryos under tunicamycin

Three independent experiments were conducted to monitor HSP-4 expression and localization in live embryos expressing an HSP-4::GFP fusion protein (cgc SJ4005). The strain employed contains a zcIs4 reporter transgene inserted to chromosome V[82]. This reporter transgene expresses an exogenous HSP-4 protein that is linked to a GFP fluorophore and is unlinked to the intrinsic HSP-4 gene found on chromosome II. Previous studies show the strain displays a strong GFP signal in gut and hypodermal cells when subjected to heat stress or tunicamycin indicating its usefulness as a marker for ER stress[77]. Worms from strain SJ4005 were moved to *icd-1, icd-2* and a control *unc-22* RNAi plates. 30 worms were maintained on each RNAi plates for 48 hours and were then moved to tunicamycin plates for imaging. Worms were grown in the tunicamycin

plates at standard laboratory conditions for 48 hours. Imaging was performed at 12 hour intervals throughout the duration of the experiment. During imaging intervals, randomly picked embryos were mounted to glass microscope slides and viewed using the Z-stack function of an inverted laser scanning confocal microscope (Nikon C1) at 60x magnification. Laser excitation and digital image capturing conditions were comparable in the three treatments to minimize variability amongst the generated Z-stacks.

2.6.1 Quantification of HSP-4 expression in ICD-1, ICD-2 and UNC-22 depleted live embryos under tunicamycin

Fluorescent Z-stack 3-D images of live embryos expressing HSP-4 were captured with an inverted laser scanning confocal microscope (Nikon C1). Images were captured using laser scanning optical microscopy and analyzed with ImageJ software as established in previous experiments[78]. Fluorescent intensity was measured with the Z-project summation function. This function sums the pixel intensity of all of the stacks and outputs a 2-D image representative of the fluorescence pixel intensity of the entire embryo. To quantify pixel intensity in the summed 2-D image, embryos were outlined and converted to 8-bit gray scale using the type submenu within the image menu. After defining the entire embryo as the region of interest, average pixel intensity was obtained using the measure tool within the analyze menu. This measurement outputs average fluorescent intensity from each pixel within the region of interest. Quantification was performed in 15-30 embryos for each imaging time interval.

2.6.2 Statistical analysis of HSP-4 expression in ICD-1, ICD-2 and UNC-22 depleted live embryos

Average pixel intensities from the three RNAi treatments under tunicamycin were exported to Statistical Analysis Systems (SAS) software. To determine the presence of a time-treatment effect, a repeated measures analysis of variance (ANOVA) was performed as established in previous experimnts[79]. To find statistically significant differences amongst treatments during each imaging interval, the repeated measures ANOVA was followed by a LSD post-hoc analysis using a significance level α of 0.05.

2.7 Monitoring increased lysosomal content in ICD-1, ICD-2 and UNC-22 depleted live embryos under tunicamycin

Three independent experiments were conducted to monitor increased lysosomal content in live embryos. Lysosomal granules possess a naturally occurring autofluorescent property when excited with an external fluorescence light source due to the protein and lipid contents contained therein[81]. Unlike signal originating from artificially added fluorophores, the natural light emission arises from intrinsic lysosomal properties and may be captured using a blue fluorescent filter. Due to this innate biological property, increased lysosomal content was assessed in progeny of worms from strain SJ4005. 30 gravid worms were fed *icd-1*, *icd-2* and a control *unc-22* RNAi for 48 hours. Following RNAi treatment, worms were moved and maintained in tunicamycin plates for 48 hours. Imaging was performed in 12 hour intervals throughout the duration of the experiment. At each imaging interval, randomly picked embryos were mounted to microscope glass slides and examined with a Zeiss Axioskop up-right fluorescence microscope at 100x magnification using a blue fluorescence filter. External fluorescence power source excitation and digital capturing conditions were comparable in the three treatments to minimize variability amongst the generated images.

2.7.1 Quantification of increased lysosomal content in ICD-1, ICD-2 and UNC-22 depleted live embryos under tunicamycin

2-D images of autofluorescing lysosomes in live embryos were captured with a Zeiss Axioskop up-right fluorescence microscope. Images were captured using brightfield optics and analyzed with ImageJ software. Pixel intensity quantification of the 2-D images was comparable to HSP-4 expression quantification and was performed in 15-30 samples for each imaging time interval.

2.7.2 Statistical analysis of increased lysosomal content in ICD-1, ICD-2 and UNC-22 live embryos

Average pixel intensities from the three RNAi treatments under tunicamycin were exported to Statistical Analysis Systems (SAS) software. The data were subjected to identical statistical analysis as HSP-4 expression.

2.8 Monitoring Fluorescence Recovery After Photobleaching (FRAP) under tunicamycin

Fluorescence Recovery After Photobleaching (FRAP) was employed to assess the embryos ability to reconstitute protein synthesis. The protocol and quantification performed in all FRAP experiments were comparable to those of FRAP studies in live *C. elegans* embryos[80]. In this technique, the fluorescent signal of cell specific markers is photobleached using an external fluorescence power source and the recovery of novel fluorescence signal is monitored over time to provide a direct measure of translation. Three separate FRAP experiments were performed. Although methodologies and

measurements were comparable, each experiment was performed using varying worm strains (see below). For all FRAP experiments 30 gravid worms were maintained in *icd-1*, *icd-2* and a control *unc-22* RNAi plates for 48 hours. Following 48 hour depletion, worms were moved and maintained on tunicamycin plates for 12 hours. Photobleaching was performed in 15-30 randomly picked embryos mounted to microscope glass slides using a Zeiss Axioskop up-right fluorescence microscope at 100x magnification. Fluorescent signal of individual embryos was extracted using an external fluorescence power source for 4 minutes. Following photobleaching, embryos were imaged at 1, 2 and 5 hours post-photobleach to monitor recovery.

2.8.1 Neuronal Yellow Fluorescence Protein (NYFP) FRAP under tunicamycin

To examine neuronal cell's ability to reconstitute protein synthesis under tunicamycin stress, FRAP was performed in embryos containing a pan neuronal yellow fluorescence protein marker driven by an unc-119 neuronal trafficking protein promoter (cgc TU3310). Pan neuronal markers have multiple targets (somatic, nuclear, dendrites and axons) and are consequently employed as global neuronal markers. In this experiment worms were not subjected to RNAi depletion. However, adults were maintained in tunicamycin plates for 12 hours and embryo imaging was performed during the previously stated time intervals and imaging conditions. Untreated samples were obtained from worms maintained in NGM plates containing DMSO only. External fluorescence power source excitation and digital capturing conditions were comparable in the three treatments to minimize variability amongst the generated images.

2.8.2 Gut Red Fluorescence Protein (GRFP) FRAP under tunicamycin

To assess recovery of translation in gut cells under tunicamycin stress, FRAP was performed in embryos expressing a peroxisomal targeting signal-1 (PTS1) RFP fusion protein (cgc VS10). PTS1 is a ring finger protein required for import of peroxisomal matrix proteins in gut cells, therefore the RFP signal is emitted from peroxisomes in the intestinal cell lineage. Untreated samples were comparable to the NYFP FRAP under tunicamycin. Imaging conditions and acquisition were performed as stated under Monitoring Fluorescence Recovery After Photobleaching (FRAP) under tunicamycin. External fluorescence power source excitation and digital capturing conditions were comparable in the three treatments to minimize variability amongst the generated images.

2.8.3 Neuronal Yellow Fluorescence Protein (NYFP) FRAP in ICD-1 and ICD-2 depleted embryos under tunicamycin

FRAP was performed in NYFP embryos depleted of either ICD-1 or ICD-2 following 12 hour tunicamycin exposure to examine differences in protein synthesis recovery in the presence of either subunit. Imaging conditions and acquisition were performed as stated under Monitoring Fluorescence Recovery After Photobleaching (FRAP) under tunicamycin. External fluorescence power source excitation and digital capturing conditions were comparable in the three treatments to minimize variability amongst the generated images.

2.8.4 Quantification of Fluorescence Recovery After Photobleaching (FRAP) under tunicamycin

2-D fluorescence images of live embryos during recovery were captured with a Zeiss Axioskop up-rights fluorescence microscope. Images were captured using brightfield

optics and analyzed with ImageJ software. The protocol for pixel intensity quantification of the 2-D images was identical to HSP-4 expression quantification and was performed in 20-30 samples for each imaging time interval.

2.8.5 Statistical analysis of Fluorescence Recovery After Photobleaching (FRAP) under tunicamycin

The average pixel intensities generated from the FRAP images were exported to excel. A simple regression model was generated to determine the degree of correlation (R^2) amongst fluorescent signal recovery over time in the three FRAP experiments as previously established[80].

2.9 Monitoring NYFP and GRFP expression in ICD-1, ICD-2 and UNC-22 depleted live embryos under tunicamycin

Three independent experiments were conducted to monitor NYFP and GRFP expression as well as localization in live embryos expressing a unc-119::YFP (cgc TU3310) and PTS1::RFP (cgc VS10) fusion proteins, respectively[83, 84]. Experimental conditions, parameters and image acquisition performed was comparable to the above stated Monitoring HSP-4 expression in ICD-1, ICD-2 and UNC-22 depleted live embryos under tunicamycin . However, imaging was performed in live embryos from the three RNAi treatments at 12 and 24 hour tunicamycin exposure. Laser excitation and digital image capturing conditions were comparable in the three treatments to minimize variability amongst the generated Z-stacks.

2.9.1 Quantification of NYFP and GRFP expression in ICD-1, ICD-2 and UNC-22 depleted live embryos under tunicamycin

Fluorescent Z-stack 3-D images of live embryos were captured with a Nikon C1 inverted laser scanning confocal microscope. Images were captured using laser scanning optical microscopy and analyzed using the Z-project summation function of the ImageJ software as previously established[78]. Fluorescent intensity of the summed 2-D images was quantified as previously stated under Quantification of HSP-4 expression in ICD-1, ICD-2 and UNC-22 depleted live embryos under tunicamycin and was performed in 15-30 samples for each imaging time interval.

2.9.2 Statistical analysis of NYFP and GRFP expression in ICD-1, ICD-2 and UNC-22 depleted live embryos under tunicamycin

Average pixel intensities of the three RNAi treatments under tunicamycin generated from the NYFP and GRFP summed images were exported to Statistical Analysis Systems (SAS) software. The pooled data from the experiments conducted in the two strains were subjected to identical statistical analysis as HSP-4 expression[79].

3 Results

3.1 effect of tunicamycin exposure on adult worm viability

Exposure to tunicamycin, an antibiotic isolated from *Streptomyces*, elicits an ER-specific UPR by inhibiting N-linked glycosylation of proteins being processed for secretion or membrane localization. Previous experiments show that, relative to ICD-1 depletion, ICD-2 depleted adult worms are more resistant to heat stress as measured by survival[62]. To determine whether worms depleted of ICD-1 or ICD-2 display altered viability under sustained ER stress, survival of adult nematodes exposed to tunicamycin was measured in samples depleted of either protein subunit as well as a control treatment. Interestingly, a greater proportion of ICD-1 depleted worms were more resistant to death in the presence of tunicamycin relative to ICD-2 and UNC-22 depleted worms throughout the length of the experiment. In addition, *icd-2* and *unc-22* RNAi treatments displayed virtually equal proportions of viable nematodes during 24 and 36 hour tunicamycin exposures (Figure 1).

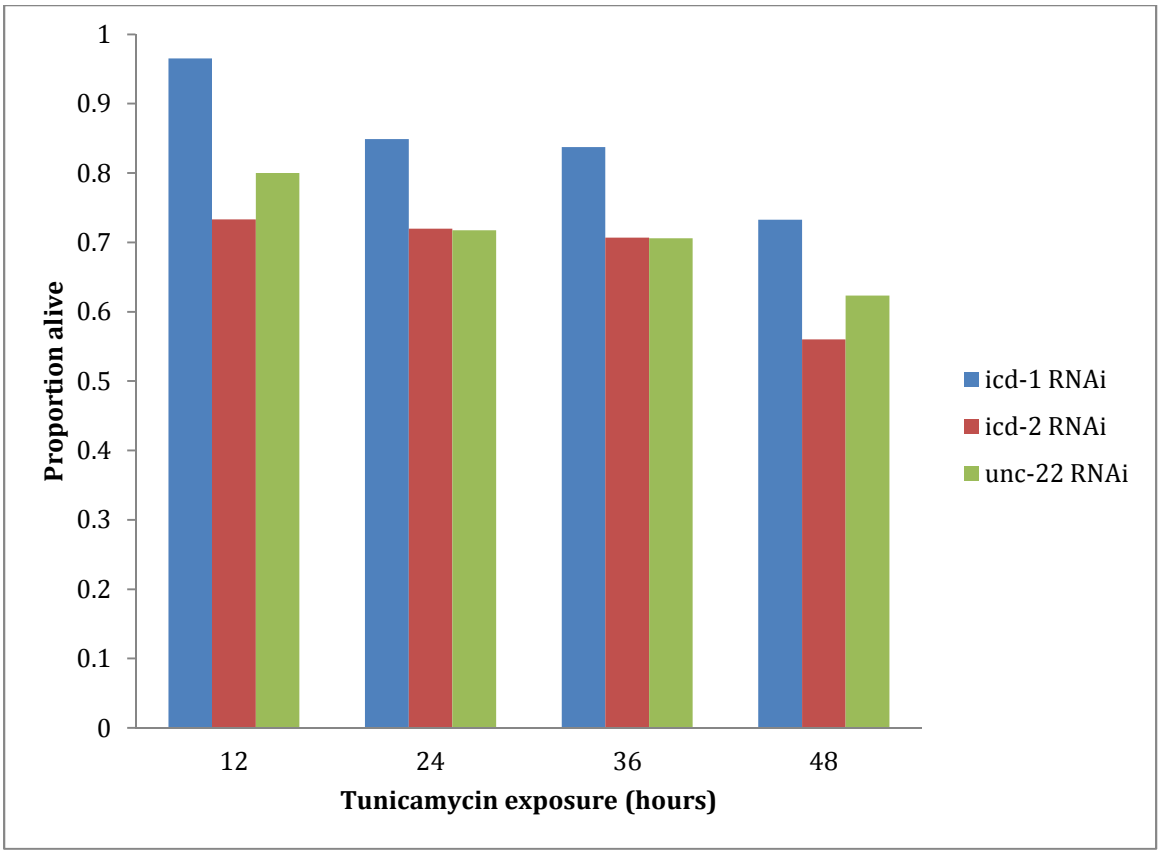

Figure 1: **Proportion of alive adult *C. elegans* under tunicamycin exposure following *icd-1*, *icd-2* and *unc-22* RNAi.** Gravid adults were exposed to tunicamycin for a duration of 48 hours. Viability was measured every 12 hours by pharyngeal pumping in response to prodding with a heated platinum pick. Treatment worms were maintained in RNAi plates for 48 hours prior to tunicamycin exposure (n = 20-30 adults for each measured time point).

3.2 ICD-1 depletion leads to greater induction of HSP-4 chaperone expression relative to ICD-2 and UNC-22 depletion during sustained ER stress

Independent studies, employing distinct model systems, show that depletion of either NAC subunit is sufficient to activate the ER specific UPR[62, 63]. To determine whether the increased viability of ICD-1 depleted worms in the presence of tunicamycin was a result of ER specific chaperone up-regulation, HSP-4 levels were monitored in embryos obtained from adults fed *icd-1*, *icd-2* or *unc-22* RNAi for 48 hours prior to tunicamycin exposure for 12 and 24 hours. Given that HSP-4 is the *C. elegans* homologue of the mammalian ER chaperone BiP, an HSP-4::GFP reporter strain was employed to quantify ER specific chaperone levels (see methods).

At 12 hour tunicamycin exposure, ICD-1 depleted embryos displayed a large increase in HSP-4::GFP reporter expression compared to ICD-2 or UNC-22 depleted embryos. Furthermore, the majority of the signal in ICD-1 depleted embryos was localized to the anterior portion of the embryo where most cells are of neuronal lineage. ICD-2 and UNC-22 depleted embryos displayed similar HSP-4::GFP localization, with weak expression at the anterior portion of the embryo. The neuronal HSP-4::GFP expression obtained in all RNAi experimental populations when exposed to tunicamycin was absent in untreated wild-type embryos (Figure 2 A.)

24 hour tunicamycin exposure also led to a large increase in HSP-4::GFP reporter expression in ICD-1 depleted embryos relative to ICD-2 or UNC-22 depleted embryos. However, the HSP-4::GFP signal in ICD-1 depleted embryos expanded from the anterior portion of the embryo to the posterior region during the 24 hour tunicamycin-imaging interval. Similarly, the ICD-2 and UNC-22 depleted embryos displayed a stronger,

diffused, HSP-4::GFP expression in the posterior region that was absent during 12 hour tunicamycin exposure in these experimental treatments. However, only UNC-22 depleted embryos depicted an increase in HSP-4::GFP expression levels from 12 hour to 24 hour tunicamycin exposure in the anterior region. The HSP-4::GFP expression levels in ICD-2 depleted embryos seemed virtually unaltered in the anterior portion with prolonged tunicamycin exposure (Figure 2 B.).

To compare the HSP-4::GFP signal strength of ICD-1, ICD-2 and UNC-22 depleted embryos during 12 and 24 hour tunicamycin exposure, the fluorescent intensity of randomly picked embryos from each respective experimental population was quantified. Although all experimental populations displayed an increase in HSP-4::GFP signal relative to untreated embryos (- tunicamycin), RNAi treatment specific differences were observed at both 12 and 24 hour tunicamycin exposure. On average, the HSP-4::GFP fluorescent intensity at 12 hour tunicamycin exposure in ICD-1 depleted embryos was 4 times greater than ICD-2 depleted embryos and 1.5 times greater than control embryos (Figure 3). Given that a repeated measures ANOVA yielded a significant time and treatment difference ($P < 0.05$), an LSD and Tukey post-hoc analysis was performed. The LSD analysis minimizes type-2 error rate whereas Tukey analysis minimizes type-1 error rate. For 12 hour tunicamycin exposure, LSD analysis revealed all averages where significantly different from each other ($P < 0.05$). However, the results from a more conservative Tukey analysis showed the average fluorescent intensity in ICD-2 depleted embryos was significantly lower than the average fluorescent intensity of ICD-1 depleted embryos and control embryos, which were not significantly different from each other ($P < 0.05$) (Figure 3). Consistent with the signal strength pattern obtained at 12 hour

tunicamycin exposure, the average fluorescent intensity was strongest in ICD-1 depleted embryos followed by controls and lowest in ICD-2 depleted embryos. Overall, there was an increase in average fluorescent intensity in all treatments with sustained tunicamycin exposure. On average, the HSP-4::GFP fluorescence intensity at 24 hour tunicamycin exposure in ICD-1 depleted embryos was 3.5 times greater than ICD-2 depleted embryos and 2 times greater than control embryos. During 24 hour tunicamycin exposure, the results from both LSD and Tukey post-hoc analysis showed the average fluorescent intensity in ICD-1 depleted embryos was significantly higher than the average fluorescent intensity of ICD-2 depleted embryos and controls, which were not significantly different each other ($P < 0.05$) (Figure 3).

To further characterize the differences in the localization of HSP-4::GFP expression, ICD-1 and ICD-2 depleted embryos subjected to 24 hour tunicamycin exposure were carefully examined under oil immersion. The ICD-2 depleted embryos depicted a diffuse signal throughout the embryo along with a portion of the signal distinctly originating from lysosomal structures. ICD-1 depleted embryos contained a diffuse signal in the entirety of the embryo but lacked any distinct signal emerging from lysosomal structures within the embryo (Figure 4). Therefore at 12 and 24 hour tunicamycin exposure, ICD-1 and ICD-2 depleted embryos varied in HSP-4::GFP localization, abundance and source of signal.

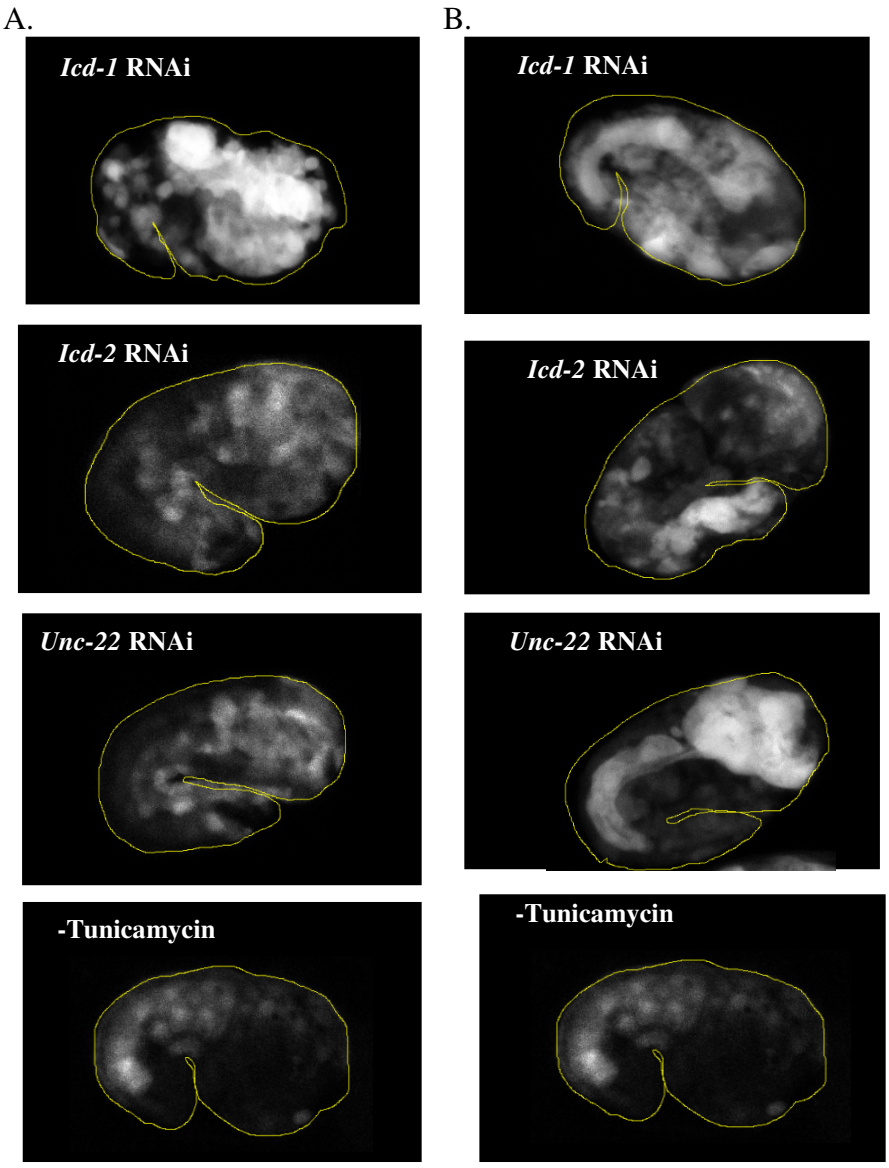

Figure 2: **3D projection of HSP-4::GFP expression in *icd-1*, *icd-2* or *unc-22* RNAi treated adults exposed to tunicamycin as well as untreated samples.** Images were acquired under 60x magnification and identical exposure settings using a Nikon C1 inverted laser scanning confocal microscope. 3D projections were generated using the Z-project summation tool in ImageJ. Following 48 hour *icd-1*, *icd-2* or *unc-22* RNAi, parental worms were exposed to tunicamycin. Randomly picked embryos from each RNAi experimental population under tunicamycin were mounted on agar pads and imaged at 12 hour tunicamycin exposure (Images on column A) as well as 24 hour tunicamycin exposure (Images on column B). Untreated embryos were also imaged for comparison (Image A and B). Embryos in images A and B were genetically identical, containing an HSP-4::GFP reporter construct (cgc SJ4005).

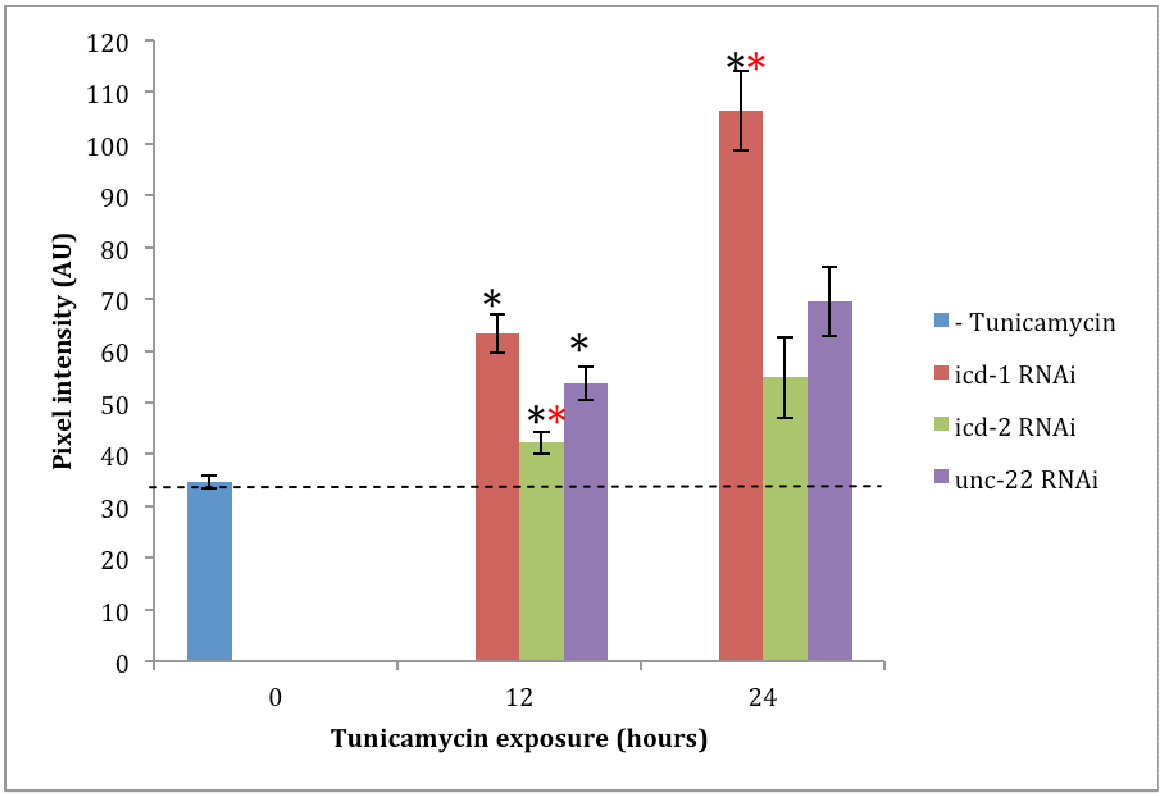

Figure 3: **Quantified average HSP-4::GFP fluorescent intensity of whole embryos obtained from *icd-1*, *icd-2* and *unc-22* RNAi treated adults exposed to tunicamycin.** The HSP-4::GFP fluorescent intensity of 3D projections generated from *icd-1*, *icd-2* and *unc-22* depleted embryos during 12 and 24 hour tunicamycin exposure was quantified using the Z-project summation function in ImageJ. Each bar represents the average pixel intensity (AU) for all embryos in each experimental population. The error bars represent standard error for each average pixel intensity. A repeated measures ANOVA followed by a LSD and Tukey post-hoc analysis was performed using SAS. * denotes significant difference of $P < 0.05$ for LSD analysis and * denotes significant difference of $P < 0.05$ for Tukey analysis. Average HSP-4::GFP pixel intensity of untreated embryos (- tunicamycin) was also presented for comparison to basal signal strength (n = 15-30 embryos for each measured time point).

A.

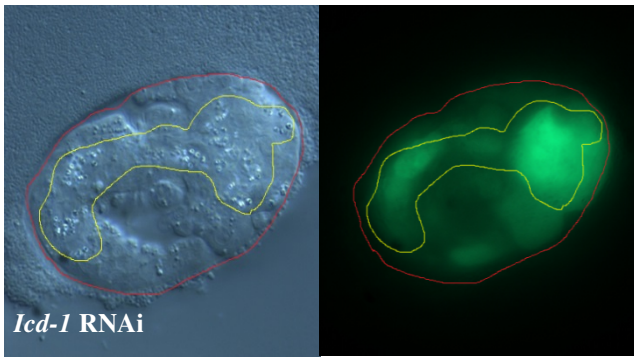

B.

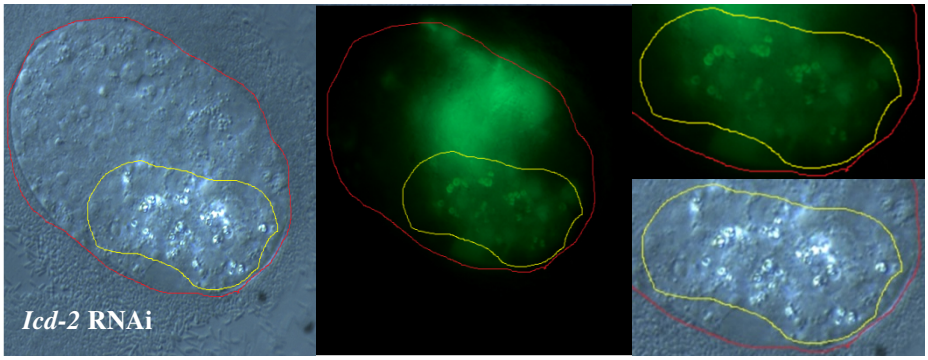

Figure 4: **Comparison of HSP-4::GFP signal source in ICD-1 and ICD-2 depleted embryos during tunicamycin exposure.** Images were acquired under 100x magnification and identical exposure settings using a Zeiss Axioskop up-right fluorescence microscope. Following 48 hour ICD-1 or ICD-2 depletion, parental worms were exposed to 24 hour tunicamycin. Randomly picked embryos from the *icd-1* RNAi (A.) and *icd-2* RNAi (B.) experimental population under tunicamycin were mounted on agar pads and imaged at 24 hour tunicamycin exposure.

3.3 ICD-1, ICD-2 and UNC-22 depletion leads to equivalent levels of lysosomal presence during sustained ER stress

After confirming that HSP-4::GFP expression was significantly higher in ICD-1 depleted embryos relative to ICD-2 depleted embryos exposed to tunicamycin, differences in lysosomal presence were assessed to determine whether the observed increase in UPR activity leads to an increase in protein turnover in ICD-1, ICD-2 or UNC-22 depleted embryos under tunicamycin. Lysosomal granules possess a naturally occurring autofluorescent property when excited with a blue fluorescence light source due to the protein and lipid contents contained within the lysosome. Due to this innate biological property, differences in lysosomal presence were able to be assessed in the progeny of adults containing an HSP-4::GFP reporter. Adult nematodes were fed *icd-1*, *icd-2* or *unc-22* RNAi for 48 hours prior to tunicamycin exposure for 12 and 24 hours. All of the RNAi experimental populations exhibited a minor qualitative increase in the abundance, size and localization of the auto fluorescent lysosomal granules relative to untreated samples during both 12 and 24 hour tunicamycin exposure (data not shown).

Given that the differences in increased lysosomal generation appeared to be negligible between treatment populations while qualitatively different when compared to untreated, the autofluorescent lysosomal intensity of randomly picked embryos from each respective experimental population was quantified and compared to untreated. The average auto fluorescent lysosomal pixel intensity appeared to increase in ICD-1 and ICD-2 depleted embryos relative to untreated samples during 12 hour tunicamycin exposure. In contrast, UNC-22 depleted embryos failed to display an increased lysosomal generation during 12 hour tunicamycin exposure. On average, after 24 hours

of tunicamycin exposure, all RNAi treatments appeared to display an increased lysosomal generation relative to basal autofluorescent lysosomal pixel intensity. However, results from a repeated measures ANOVA revealed there were no significant differences in increased lysosomal generation between ICD-1, ICD-2 or UNC-22 depleted embryos during 12 and 24 hour tunicamycin exposure ($P > 0.05$) (Figure 5).

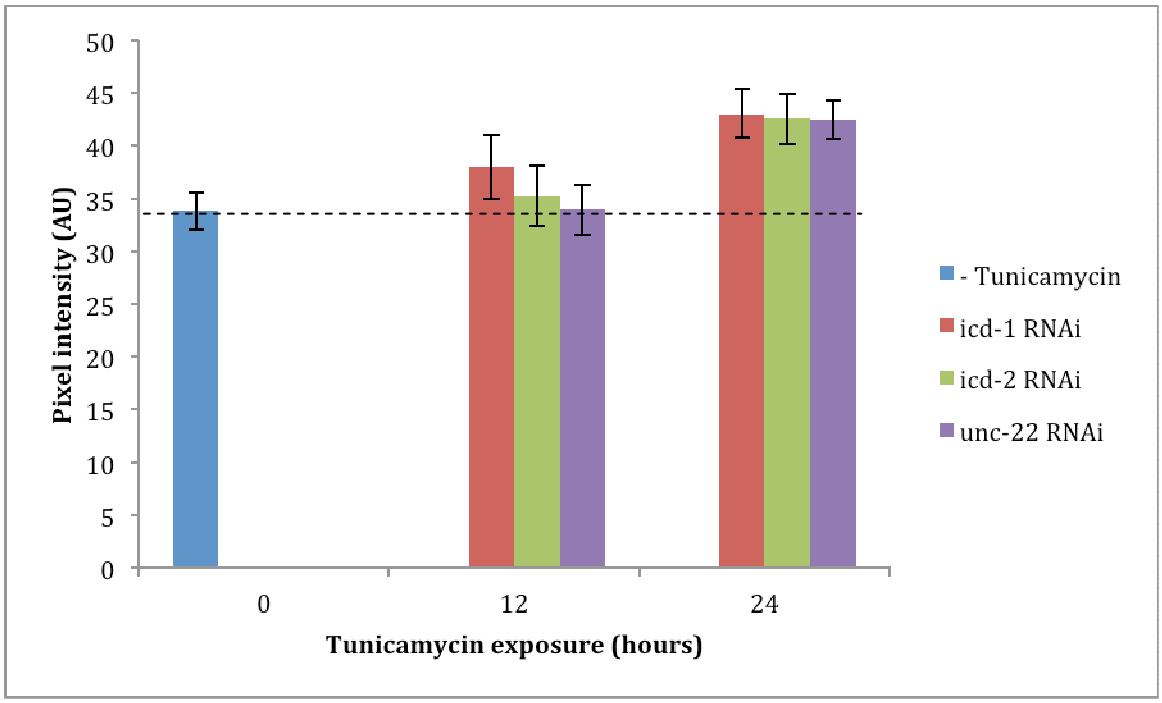

Figure 5: **Quantified average Lysosomal autofluorescent intensity of whole embryos obtained from *icd-1*, *icd-2* and *unc-22* RNAi treated adults exposed to tunicamycin.** The auto fluorescent lysosomal intensity of single plane images from ICD-1, ICD-2 and UNC-22 depleted embryos during 12 and 24 hour tunicamycin exposure were quantified using ImageJ. Each bar represents the average pixel intensity (AU) for all embryos in each experimental population. The error bars represent standard error for each average pixel intensity. Average auto fluorescent lysosomal pixel intensity of untreated embryos (- tunicamycin) was also presented for comparison to basal signal strength (n = 15-30 embryos for each measured time point).

3.4 ICD-1-depleted embryos display a more robust attenuation of protein synthesis compared to ICD-2-depleted embryos during ER stress

Although neither ICD-1 nor ICD-2 depleted embryos under ER stress failed to show significant differences in lysosomal presence (Figure 5), statistical analysis showed ICD-1-depleted embryos exhibited a greater HSP-4::GFP signal during 12 and 24 hour tunicamycin exposure compared to ICD-2-depleted embryos under similar stress (Figure 3). Based on the results obtained after assessing two major UPR outcomes, fluorescence recovery after photo bleaching (FRAP) was employed to explore levels of protein synthesis attenuation during ER stress, another important cell-saving stress response. An advantage in this procedure is the presence of cell-type specific fluorescent proteins that allowed for FRAP to be conducted in transgenic embryos expressing a pan neuronal yellow fluorescent protein (YFP) (TU3310) as well as embryos expressing a gut cell red fluorescent protein (RFP). In these embryos, FRAP was performed in ICD-1 or ICD-2 depleted populations under ER stress to correlate differences in protein production with varying levels of α or βNAC. Embryos were acquired from adult worms subjected to 12 hour tunicamycin exposure, previously established as sufficient to elicit an increase in HSP-4::GFP levels in all RNAi treatments relative to untreated embryos (figure 3).

In the – tunicamycin and + tunicamycin neuronal YFP experimental populations, a 4 minute photo bleach was sufficient to eliminate any detectable signal (Figure 6). Following a 5 hour recovery, untreated samples displayed a diffuse YFP signal throughout the entire embryo (Figure 6A). However, the neuronal YFP signal in the tunicamycin -treated embryos appeared to originate solely from a specific region of the embryo that will eventually give rise to the head portion of the adult worm (Figure 6B).

To confirm the apparent difference in recovery amongst the two samples, YFP pixel intensities were quantified for each treatment at specified time points throughout the duration of the experiment and a regression analysis of the average pixel intensities over time was performed. Tunicamycin -treated samples retained relatively equal YFP average pixel intensities throughout the recovery period and failed to reconstitute pre-photo bleach average pixel intensity (Figure 7A). Untreated samples displayed a gradual increase in YFP average pixel intensity during the recovery period but also failed to reach the initial average pixel intensity (Figure 7A). The regression analysis revealed a strong positive linear trend in signal recovery over time in the untreated samples, which was absent in the tunicamycin treated samples (Figure 7B).

Like both neuronal YFP populations, 4 minutes of photo bleaching eliminated any detectable signal in gut cell RFP embryos (Figure 8). Unlike the neuronal YFP embryos, both treated and untreated embryos displayed virtually equal gut cell RFP expression patterns following a 5 hour recovery (Figure 8). Quantified RFP pixel intensity showed both treatments almost reached their respective initial pre-photo bleach average pixel intensity following a 1 hour recovery (Figure 9A). Furthermore, a 5 hour recovery period led to virtually identical average pixel intensities in both treated and untreated samples (Figure 9A.) A regression analysis of the quantified GRFP average pixel intensity revealed both GRFP sample populations displayed similar linear trends in signal recovery throughout the recovery period (Figure 9B.).

After characterizing protein synthesis changes in two stressed nematode strains containing cell specific markers and fully functional NAC, attenuation of protein synthesis during ER stress was assessed in neuronal YFP transgenic embryos depleted of

either ICD-1 or ICD-2. In ICD-1 or ICD-2 depleted embryos exposed to tunicamycin (12 hours), a 4 minute photo bleach successfully reduced initial YFP pixel intensity levels (Figure 10). Although ICD-1 and ICD-2 depleted embryos were subjected to identical tunicamycin exposure times, the two sample populations displayed distinct YFP signal expression patterns; the neuronal marker signal in ICD-1 depleted embryos appeared confined to a specific region of the embryo, whereas ICD-2 defective embryos displayed a diffuse YFP signal throughout the entire embryo along with some signal confined to the similar region observed with ICD-1 depletion (Figure 10). To reinforce this striking observation, a regression analysis of the quantified neuronal YFP average pixel intensities throughout the recovery period was performed. Consistent with previous results, tunicamycin -treated ICD-1 defective embryos retained relatively equal YFP average pixel intensities throughout the recovery period and failed to reconstitute initial average pixel intensity (Figure 11A.). Alternatively, tunicamycin -treated ICD-2 defective embryos portrayed a gradual increase in YFP average pixel intensities throughout the recovery period and reached nearly equal pre-photo bleach average pixel intensity (Figure 11A.). In addition, a regression analysis revealed the rate of protein synthesis was quicker with ICD-2 depletion relative to ICD-1 depletion (Figure 11B). Therefore, in the presence of ER stress, ICD-2 depleted embryos interestingly mimicked the FRAP profile of untreated neuronal YFP embryos while YFP recovery in ICD-1 depleted embryos was consistent with tunicamycin-treated neuronal YFP embryos.

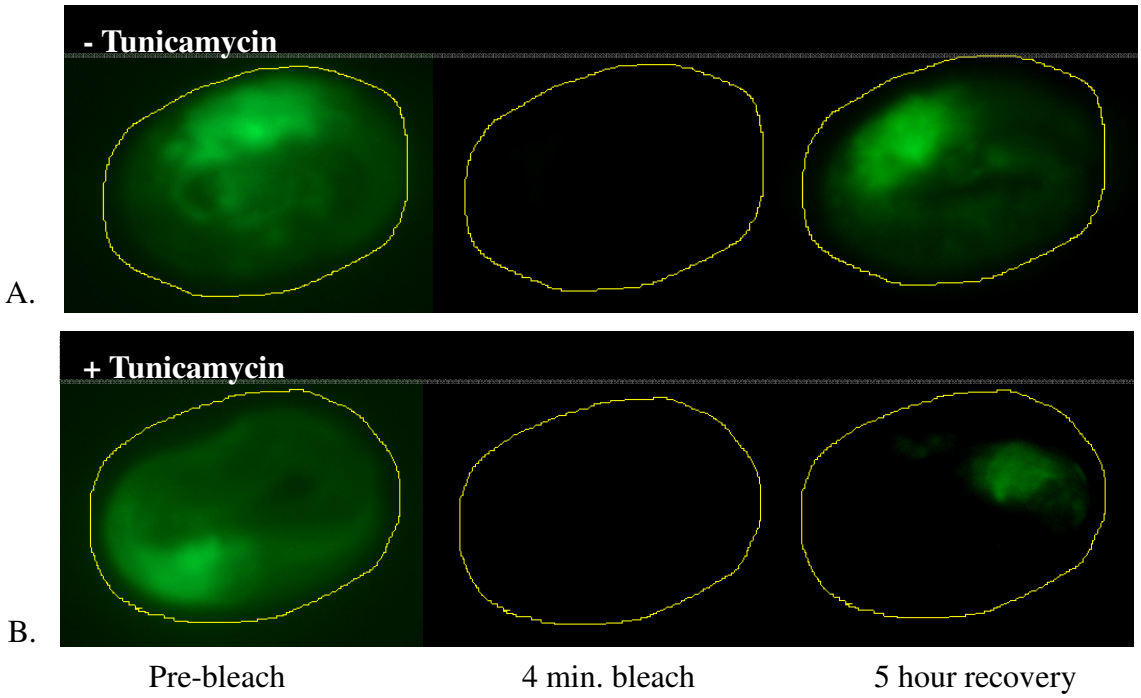

Figure 6: **Comparison of pan neuronal YFP FRAP recovery profile in tunicamycin treated and untreated embryos.** Images were acquired under 100x magnification and identical exposure settings using a Zeiss Axioskop up-right fluorescence microscope. Untreated samples were obtained from worms maintained in NGM plates containing DMSO only (A). tunicamycin treated samples were subjected to a 12 hour stress period (B). Embryos were mounted on agar pads at each imaging interval. Fluorescent signal of individual embryos was extracted using an external fluorescence power source for a duration of 4 minutes. Following photo bleaching, recovery was monitored by imaging embryos at 1, 2 and 5 hours post-photo bleach. Embryos in images A and B were genetically identical, containing pan neuronal YFP reporter construct (cgc TU3310).

A.

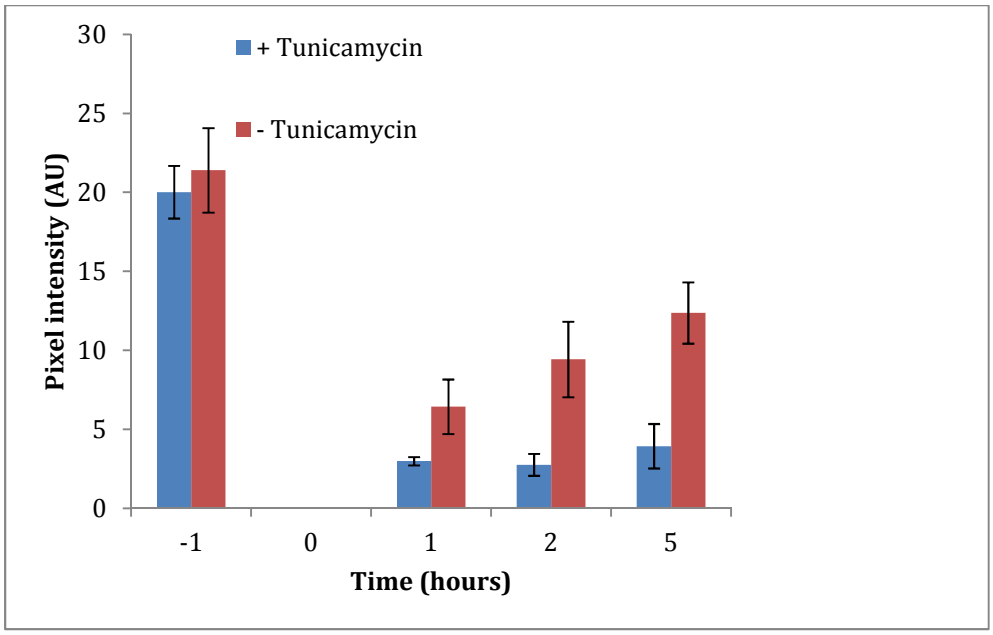

B.

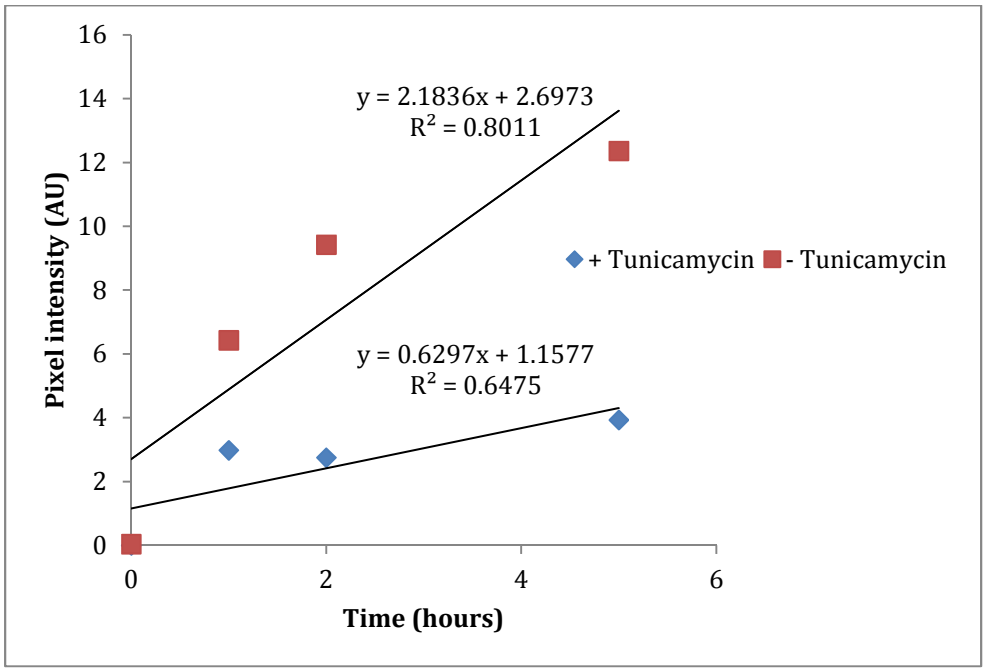

Figure 7: **Quantification and regression analysis of pan neuronal YFP recovery in tunicamycin treated and untreated embryos.** NYFP pixel intensity of single plane images from untreated and 12 hour tunicamycin treated embryos was quantified using ImageJ. Each bar represents the average pixel intensity (AU) during each imaging interval and error bars represent standard error for each average pixel intensity (Image A). A regression analysis of the average pixel intensity during each imaging interval was performed using Microsoft excel (Image B) (n = 15-30 embryos for each measured time point).

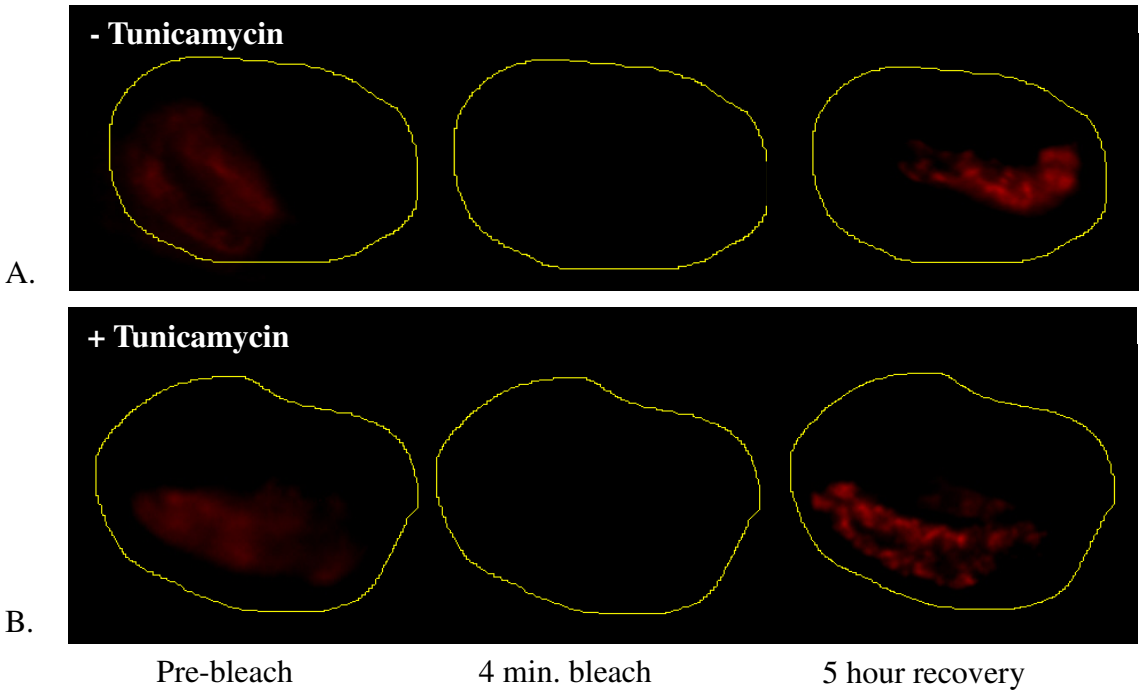

Figure 8: **Comparison of gut cell RFP FRAP recovery profile in tunicamycin treated and untreated embryos.** Images were acquired under 100x magnification and identical exposure settings using a Zeiss Axioskop up-right fluorescence microscope. Untreated samples were obtained from worms maintained in NGM plates containing DMSO only (A). Tunicamycin treated samples were subjected to a 12 hour stress period (B). Embryos were mounted on agar pads at each imaging interval. Fluorescent signal of individual embryos was extracted using an external fluorescence power source for a duration of 4 minutes. Following photo bleaching, recovery was monitored by imaging embryos at 1, 2 and 5 hours post-photo bleach. Embryos in images A and B were genetically identical, containing gut cell specific peroxisomal RFP reporter construct (cgc VS10).

A.

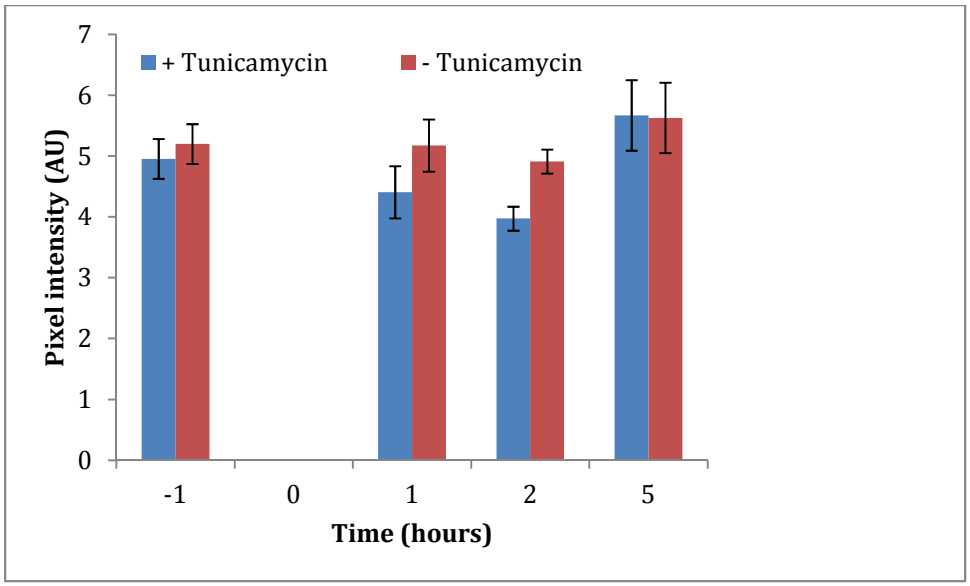

B.

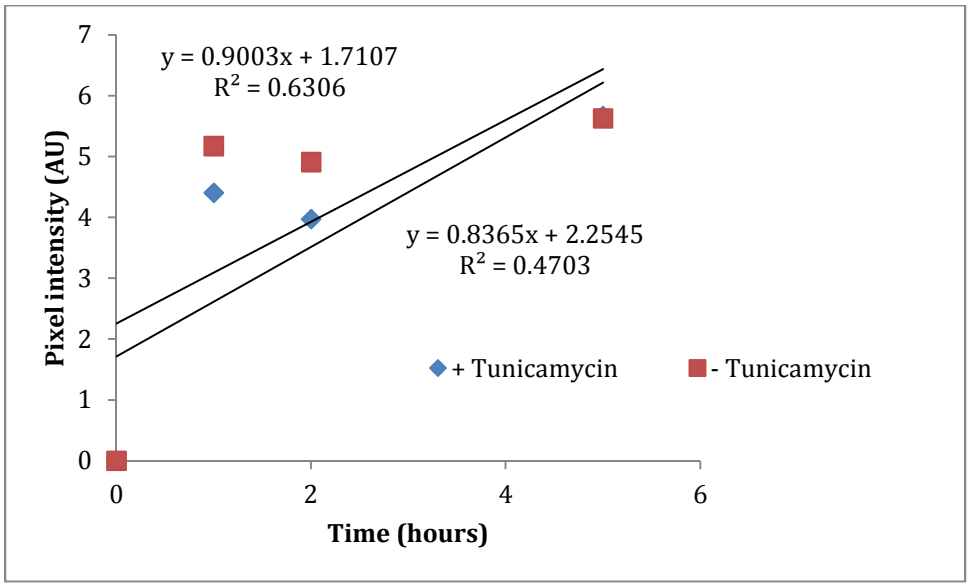

Figure 9: **Quantification and regression analysis of gut cell RFP recovery in tunicamycin treated and untreated embryos.** GRFP pixel intensity of single plane images from untreated and 12 hour tunicamycin treated embryos was quantified using ImageJ. Each bar represents the average pixel intensity (AU) during each imaging interval and error bars represent standard error for each average pixel intensity (A). A regression analysis of the average pixel intensity during each imaging interval was performed using Microsoft excel (B) (n = 15-30 embryos for each measured time point).

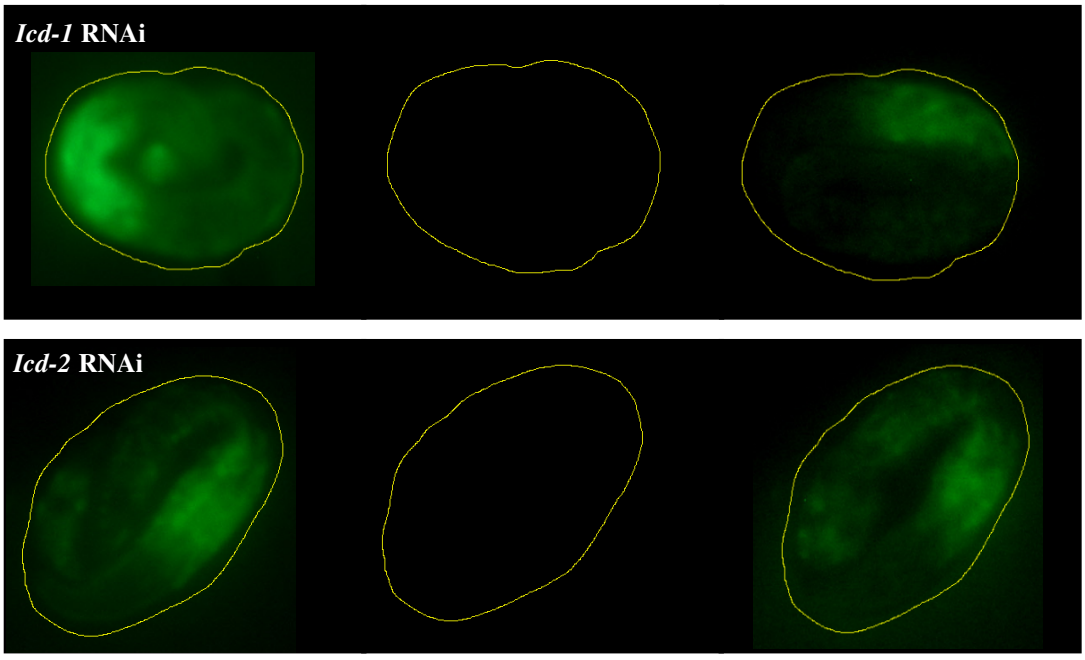

Figure 10: **Comparison of pan neuronal YFP FRAP recovery profile in ICD-1 or ICD-2 depleted embryos exposed to tunicamycin.** Images were acquired under 100x magnification and identical exposure settings using a Zeiss Axioskop up-right fluorescence microscope. Following 48 hour ICD-1 or iICD-2 depletion, embryos were subjected to 12 hour tunicamycin exposure. Embryos were mounted on agar pads at each imaging interval. Randomly picked embryos depleted of either ICD-1 (Image A) or ICD-2 (Image B) were mounted on agar pads and imaged at 12 hour tunicamycin exposure. Embryos in images A and B were genetically identical, containing pan neuronal YFP reporter construct (cgc TU3310).

A.

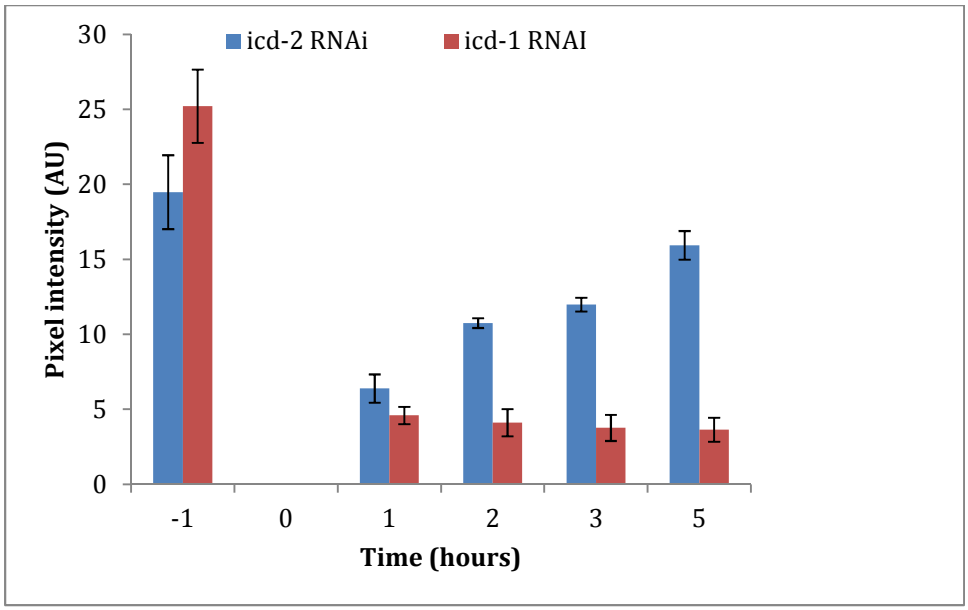

B.

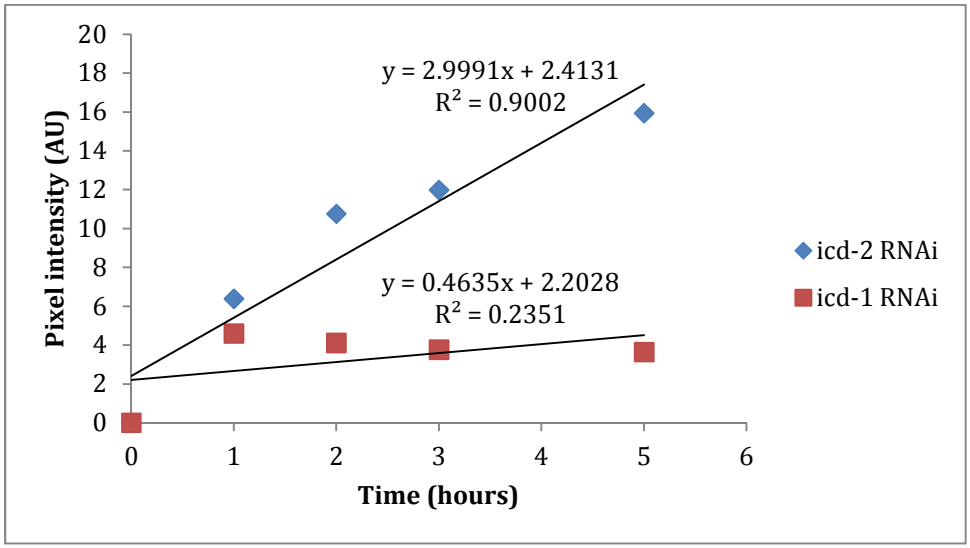

Figure 11: **Quantification and regression analysis pan neuronal YFP FRAP recovery profile in ICD-1 or ICD-2 depleted embryos exposed to tunicamycin.** NYFP pixel intensity of single plane images from ICD-1 or ICD-2 depleted embryos subjected to 12 hour tunicamycin exposure was quantified using ImageJ. Each bar represents the average pixel intensity (AU) during each imaging interval and error bars represent standard error for each average pixel intensity (Image A). A regression analysis of the average pixel intensity during each imaging interval was performed using Microsoft excel (Image B) (n = 15-30 embryos for each measured time point).

3.5 Tunicamycin exposure reduces expression of a global neuronal marker in ICD-1 depleted embryos relative to ICD-2 depleted and control embryos

Independent studies in a variety of systems suggest αNAC and the UPR may contribute to cellular homeostasis; in some cases, disruption to either αNAC or the UPR function leads to altered cellular differentiation in similar cell types[68-74]. To test whether altered levels of *icd-1* or *icd-2* during ER stress affects neuronal development, expression of a pan neuronal marker was monitored and quantified in ICD-1, ICD-2 or UNC-22 depleted embryos under ER stress. Samples were classified as either early stage or late stage embryos to minimize developmental stage specific variation. Average neuronal YFP pixel intensity in early embryos was lower for all RNAi sample populations at 12 and 24 hour tunicamycin exposure compared to basal YFP average pixel intensity (Figure 12). A repeated measures ANOVA, followed by a LSD post-hoc analysis, revealed YFP average pixel intensity in ICD-1 depleted early embryos was significantly lower at 24 hour tunicamycin exposure relative to ICD-2 and UNC-22 defective early embryos ($P < 0.05$) (Figure 12). As expected, the majority of the signal in untreated early-stage embryos was diffuse and originated anteriorly in a region populated by neurons (figure 13). During 24 hour tunicamycin exposure, neuronal YFP expression in ICD-2 and UNC-22 depleted early embryos was comparable to untreated embryos. However, neuronal YFP expression in ICD-1 defective early embryos appeared weaker, punctate and localized to specific neurons in the embryo (Figure 13).

The neuronal YFP signal intensity trend observed in late embryos subjected to ER stress was comparable to early embryos. In late embryos, 12 and 24 hour tunicamycin exposure also led to a decreased average YFP pixel intensity in all RNAi sample

populations relative to untreated YFP average pixel intensity (Figure 14). Furthermore, statistical analysis showed YFP average pixel intensity was significantly lower in ICD-1 depleted late-stage embryos at 12 hour tunicamycin exposure relative to ICD-2 and UNC-22 depleted late-stage embryos ($P < 0.05$) (Figure 14). In untreated late embryos, neuronal YFP expression appeared primarily diffused with some signal concentrated at a specific region of the embryo. During 12 hour tunicamycin exposure, YFP expression in ICD-1 depleted embryos was strikingly confined to specific neurons whereas ICD-2 and UNC-22 depleted samples appeared to mimic homeostatic NYFP expression (Figure 15). Tunicamycin exposure decreased NYFP pixel intensity in all RNAi samples with ICD-1 depleted late and early embryos displaying the greatest decrease at 12 and 24 hour, respectively.

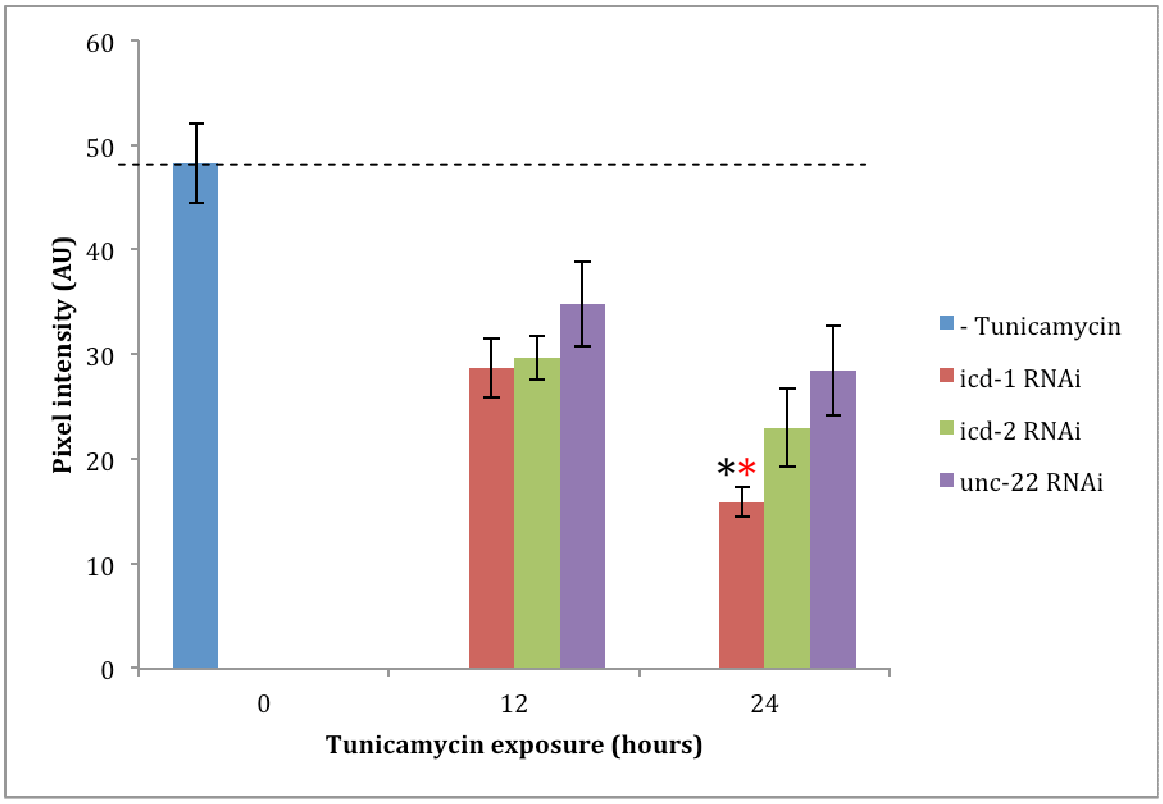

Figure 12: **Quantified average pan neuronal YFP fluorescent intensity in early embryos obtained from *icd-1*, *icd-2* and *unc-22* RNAi treated adults exposed to tunicamycin.** The NYFP fluorescent intensity of 3D projections generated from ICD-1, ICD-2 and UNC-22 depleted early embryos during 12 and 24 hour tunicamycin exposure was quantified using the Z-project summation function in ImageJ. Each bar represents the average pixel intensity (AU) for all early embryos in each experimental population. The error bars represent standard error for each average pixel intensity. A repeated measures ANOVA followed by a LSD and Tukey post-hoc analysis was performed using SAS. * denotes significant difference of $P < 0.05$ for LSD analysis and * denotes significant difference of $P < 0.05$ for Tukey analysis. Average NYFP pixel intensity of untreated early embryos (- tunicamycin) was also presented for comparison to basal signal strength (n = 15-30 embryos for each measured time point).

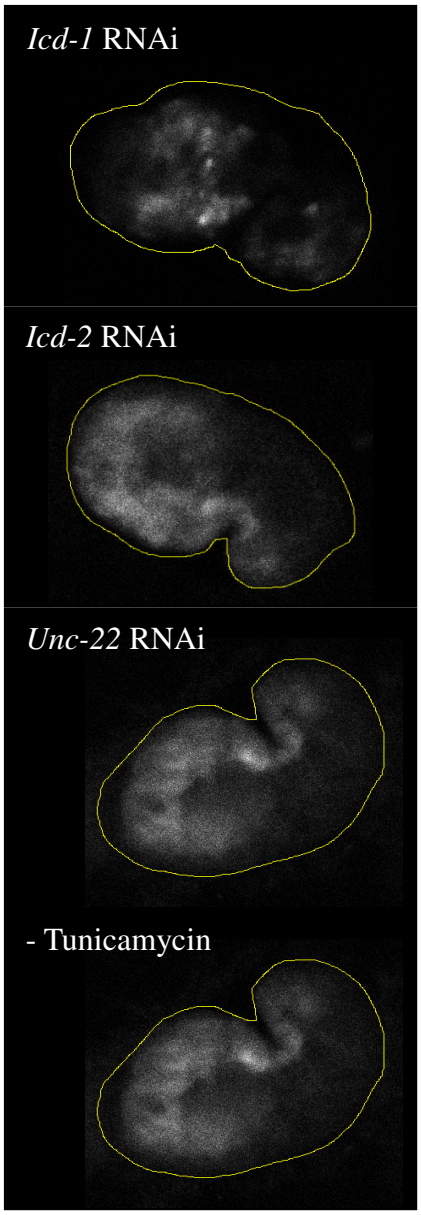

Figure 13: **3D projection of pan neuronal YFP expression in *icd-1, icd-2* or *unc-22* RNAi depleted early embryos exposed to tunicamycin as well as untreated samples.** Images were acquired under 60x magnification and identical exposure settings using a Nikon C1 inverted laser scanning confocal microscope. 3D projections were generated using the Z-project summation tool in ImageJ. Following 48 hour *icd-1*, *icd-2* or *unc-22* RNAi, parental worms were exposed to tunicamycin. Randomly picked early embryos from each RNAi experimental population under tunicamycin were mounted on agar pads and imaged at 24 hour tunicamycin exposure. Untreated early embryos were also imaged for comparison. All embryos were genetically identical, containing a pan neuronal YFP reporter construct (cgc SJ4005)

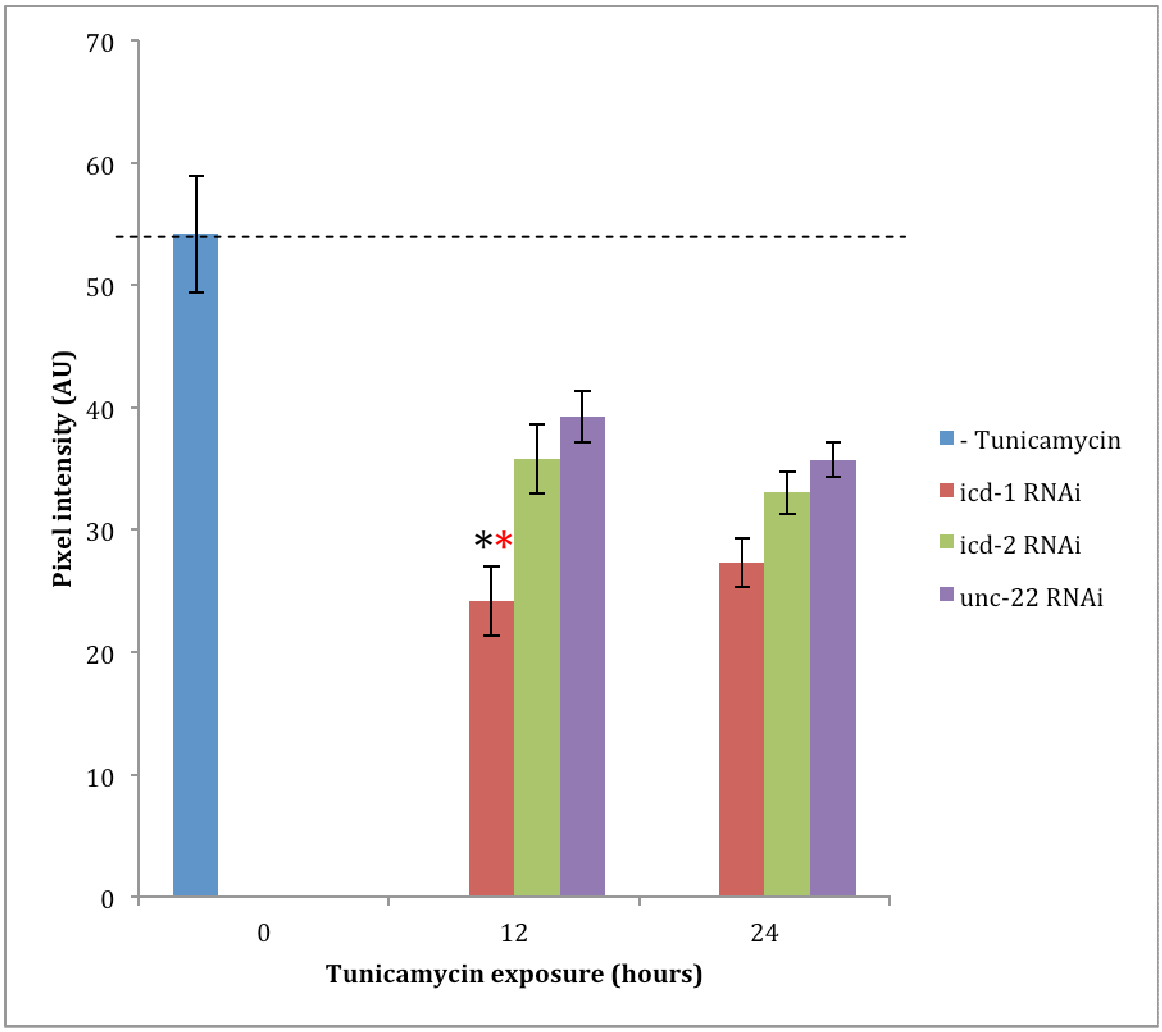

Figure 14: **Quantified average pan neuronal YFP fluorescent intensity in late embryos obtained from *icd-1*, *icd-2* and *unc-22* RNAi treated adults exposed to tunicamycin.** The NYFP fluorescent intensity of 3D projections generated from ICD-1, ICD-2 and UNC-22 depleted late embryos during 12 and 24 hour tunicamycin exposure was quantified using the Z-project summation function in ImageJ. Each bar represents the average pixel intensity (AU) for all late embryos in each experimental population. The error bars represent standard error for each average pixel intensity. A repeated measures ANOVA followed by a LSD and Tukey post-hoc analysis was performed using SAS. * denotes significant difference of $P < 0.05$ for LSD analysis and * denotes significant difference of $P < 0.05$ for Tukey analysis. Average NYFP pixel intensity of untreated late embryos (- tunicamycin) was also presented for comparison to basal signal strength (n = 15-30 embryos for each measured time point).

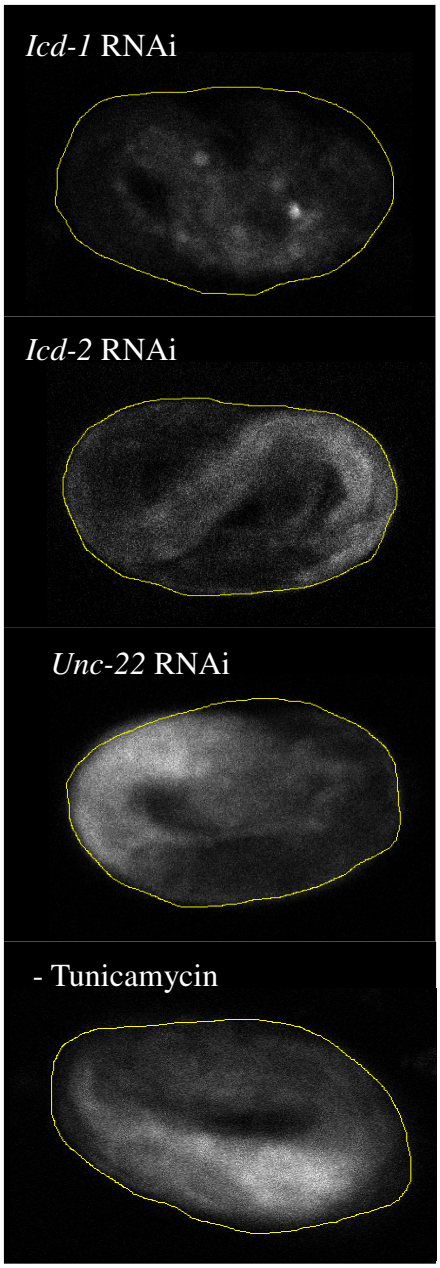

Figure 15: **3D projection of pan neuronal YFP expression in *icd-1*, *icd-2* or *unc-22* RNAi depleted late embryos exposed to tunicamycin as well as untreated samples.** Images were acquired under 60x magnification and identical exposure settings using a Nikon C1 inverted laser scanning confocal microscope. 3D projections were generated using the Z-project summation tool in ImageJ. Following 48 hour *icd-1*, *icd-2* or *unc-22* RNAi, parental worms were exposed to tunicamycin. Randomly picked late embryos from each RNAi experimental population under tunicamycin were mounted on agar pads and imaged at 12 hour tunicamycin exposure. Untreated late embryos were also imaged for comparison. All embryos were genetically identical, containing a pan neuronal YFP reporter construct (cgc SJ4005).

3.6 Tunicamycin exposure leads to equivalent expression levels of a gut cell marker in ICD-1, ICD-2 and UNC-22 depleted embryos

After finding significant differences in the expression of the specific neuronal marker employed, expression of a gut cell marker (cgc VS10) was monitored and quantified in ICD-1, ICD-2 or UNC-22 depleted embryos exposed to tunicamycin. Samples were classified into either early-stage or late-stage embryos to minimize age specific variation. 12 and 24 hour tunicamycin exposure resulted in increased gut cell RFP pixel intensity for all RNAi treatments compared to basal expression. Although ICD-1 and ICD-2 depleted early embryos depicted a gradual increase in average RFP pixel intensity, UNC-22 defective early embryos displayed a decrease in average RFP pixel intensity with sustained tunicamycin exposure. A repeated measures ANOVA showed there were no significant time and treatment differences in early-stage embryo gut cell RFP average pixel intensity ($P < 0.05$) (Figure 16). In late-stage embryos, the gut cell RFP average pixel intensities of all RNAi samples during 12 hour tunicamycin exposure was virtually equal to the average pixel intensity of untreated embryos. However, 24 hour tunicamycin exposure appeared to increase in the RFP average pixel intensity of all RNAi depleted late-stage embryos compared to untreated embryos. A repeated measures ANOVA showed there were no significant time and treatment differences in late-stage embryo gut cell RFP average pixel intensity ($P < 0.05$) (Figure 17).

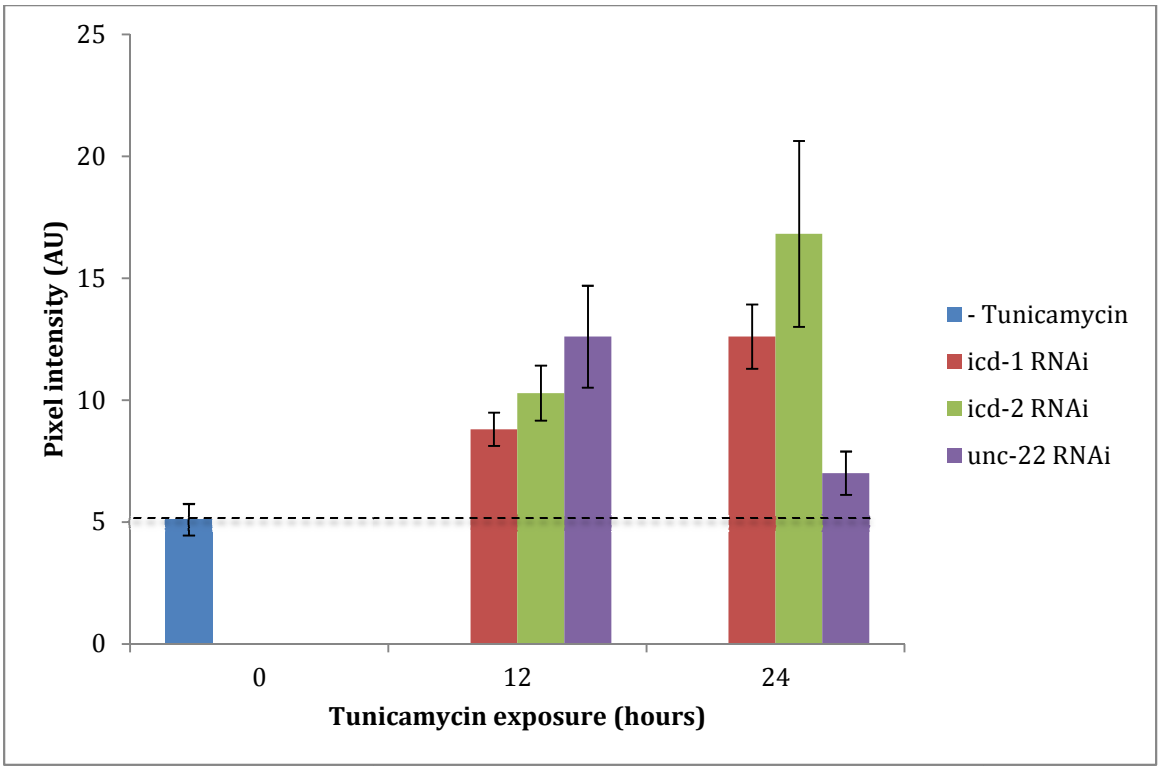

Figure 16: **Quantified average gut cell RFP fluorescent intensity in early embryos obtained from *icd-1*, *icd-2* and *unc-22* RNAi treated adults exposed to tunicamycin.** The GRFP fluorescent intensity of 3D projections generated from ICD-1, ICD-2 and UNC-22 depleted early embryos during 12 and 24 hour tunicamycin exposure was quantified using the Z-project summation function in ImageJ. Each bar represents the average pixel intensity (AU) for all early embryos in each experimental population. The error bars represent standard error for each average pixel intensity. Average GRFP pixel intensity of untreated early embryos (- tunicamycin) was also presented for comparison to basal signal strength (n = 15-30 embryos for each measured time point).

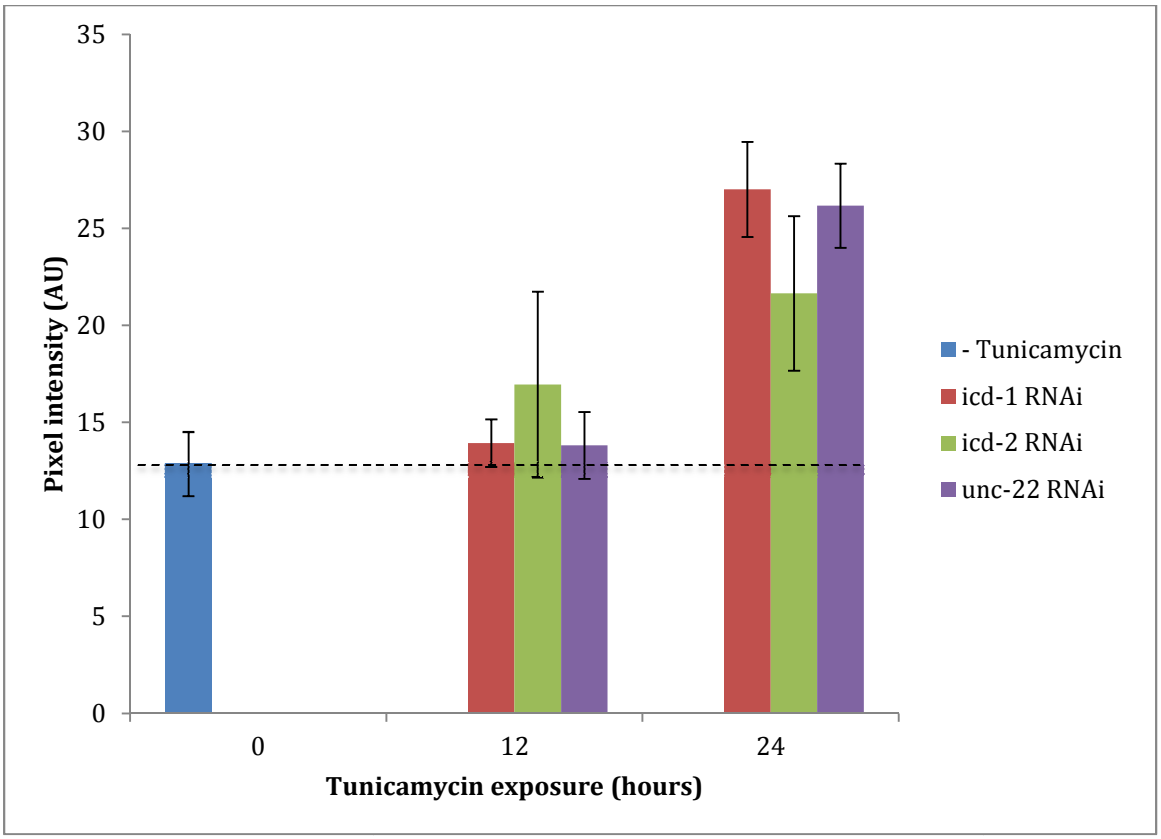

Figure 17: **Quantified average gut cell RFP fluorescent intensity in late embryos obtained from *icd-1*, *icd-2* and *unc-22* RNAi treated adults exposed to tunicamycin.** The GRFP fluorescent intensity of 3D projections generated from ICD-1, ICD-2 and UNC-22 depleted late embryos during 12 and 24 hour tunicamycin exposure was quantified using the Z-project summation function in ImageJ. Each bar represents the average pixel intensity (AU) for all late embryos in each experimental population. The error bars represent standard error for each average pixel intensity. Average GRFP pixel intensity of untreated late embryos (- tunicamycin) was also presented for comparison to basal signal strength (n = 15-30 embryos for each measured time point).

4 Discussion

The presence of a wide range of environmental stimuli (chemical agents, hypoxia, heat, inappropriate protein translocation and alterations to protein metabolism) is sufficient to induce misfolded protein stress in cells[1, 2]. If induced, cells possess various misfolded protein stress coping mechanisms responsible for restoring cellular integrity and maintaining proper functionality[3, 4]. In certain cases cells fail to resolve stress and trigger apoptosis resulting in the loss of cell function. Alternatively, an exaggerated protective response may cause highly damaged cells to evade apoptosis and become dangerous to the organism. Therefore misfolded protein stress responses become determinants of the "tipping point" between cell survival and death[9, 10]. In fact, various diseases have been causally associated with alterations in stress response function[11, 12]. In this context, the ER-specific UPR is a major contributor to the "tipping point" between cell survival and death during misfolded protein stress. The UPR elicits cell saving responses, e.g. increased expression of ER specific chaperones, attenuation of protein synthesis and increased protein turnover and ultimately cell killing responses, e.g. apoptosis as a function of the duration of misfolded protein stress[24-27]. Based on the importance and complexity of UPR activity, an understanding of factors that affect UPR activity will provide further insights into cellular responses in the presence of misfolded protein stress.

4.1 tunicamycin exposure leads to differences in ER specific chaperone expression, translation attenuation but not lysosomal presence in ICD-1 or ICD-2 depleted embryos

The heterodimeric NAC complex is hypothesized to regulate protein shuttling into the ER[49, 52, 53, 56]. Based on this model, disruption of the NAC may induce misfolded protein stress due to inappropriate protein localization to the ER, and therefore activate the UPR. Consistent with this model, removal of either α- or βNAC leads to the expression of several markers associated with an active UPR[62, 63]. Therefore, as a complex it is clear the NAC regulates protein homeostasis in the ER. However, studies suggest the individual subunits possess independent functions above and beyond the roles they play in complex with each other[57, 58]. As such, depletion of one subunit of the NAC could lead to a two-pronged engagement of the UPR: loss of NAC function initiating the UPR in addition to initiation of specific elements of the UPR by the subunit in relative excess in the cell. To test this hypothesis, differences in UPR outcomes were assessed in organisms depleted of either α- or β-NAC. The specific UPR outcomes assessed were: (1) increased expression of ER-specific chaperone, (2) attenuation of protein synthesis and (3) lysosomal presence as an indirect measure of protein turnover.

A previously proposed model assumes that eliminating NAC functionality, by removal of either α- or β-NAC, engages the UPR only by disrupting the routing of proteins to the ER. If true, removal of either NAC subunit would be expected to yield equivalent results with regards to stress-induced UPR outcomes, including the up regulation of ER specific chaperones. Quantification of total embryonic HSP-4::GFP showed tunicamycin treatment led to an increase from basal levels at 12 and 24 hour tunicamycin exposure (Figure 3), likely a result of expression in neurons as HSP-4 signal was absent in the neuronal region of untreated embryos (Figure 2). HSP-4::GFP pixel intensity was higher in ICD-1 depleted embryos compared to ICD-2 defective embryos at

12 and 24 hour tunicamycin exposure (Figure 3). Furthermore, some lysosomal HSP-4 signal was observed in ICD-2 depleted embryos, which was absent in ICD-1 depleted embryos (Figure 4). This observation reveals a striking difference in the source of the signal that may contribute to the resulting differences in HSP-4::GFP levels with depletion of either subunit. Initial HSP-4::GFP levels in samples depleted of either ICD-1 or ICD-2 may account for the variation in ER specific chaperones once tunicamycin -generated ER stress is present. Compared to ICD-2 depletion, ICD-1 depletion may lead to greater initial HSP-4::GFP up regulation that becomes augmented when exposed to tunicamycin. Although previous studies show that in the absence of exogenous stress ICD-1 depleted embryos up-regulate HSP-4::GFP compared to wild-type embryos[62], an experiment must be performed to determine whether average HSP-4::GFP levels are in fact greater in ICD-1 depleted embryos compared to ICD-2 defective embryos before the addition of tunicamycin.

Results using FRAP in *C. elegans* embryos showed 12 hour tunicamycin exposure was sufficient to suppress the recovery of a fluorescent neuronal marker (Figure 7) but not of a gut cell marker (Figure 9). A functional NAC is known to promote translation[57]; removal of either subunit would be predicted to yield an equal attenuation of protein synthesis under stress if individual subunit function had no effect on this outcome. Comparison of neuronal FRAP recovery profiles between ICD-1 and ICD-2-depleted embryos showed ICD-1 depletion led to a stronger suppression of protein synthesis during tunicamycin -mediated stress (Figure 11). In the presence of misfolded protein stress, the UPR suppresses translation to prevent cells from reaching proteotoxicity by sequestering GRP78/BiP away from PERK[30, 31]. Therefore GRP78/BiP levels are an

indicative of the extent to which UPR-mediated translation attenuation is engaged. In this context, the variation in translation attenuation observed between ICD-1 and ICD-2 depleted embryos may be a function of the extent to which the UPR was engaged as measured by HSP-4 levels, the *C. elegans* GRP78/BiP homologue. The relatively faster recovery of protein synthesis observed in ICD-2 depleted embryos antagonizes the protective UPR response and is likely a reflection of the weak increase in HSP-4::GFP during 12 hour tunicamycin exposure. Alternatively, the strong UPR induction measured by HSP-4::GFP levels in ICD-1 depleted embryos likely led to the notable suppression of protein synthesis under tunicamycin. To confirm that the robust translation attenuation in ICD-1 depleted embryos is due to increased HSP-4 levels, FRAP must be performed in tunicamycin -untreated embryos depleted of ICD-1 or ICD-2. This experiment would also reveal whether disruption of a functional NAC by removal of either subunit leads to equal levels of suppressed protein synthesis, indicating the difference obtained under ER stress is a result of a stronger UPR induction in the ICD-1 depleted samples. In addition, the FRAP recovery profile observed was only tested in a single pan neuronal marker. Therefore to further confirm the results obtained, identical experiments must be performed employing additional neuronal markers.

The UPR stimulates translation of ATF-4 during misfolded protein stress and studies have shown ATF-4 directly up-regulates the expression of mammalian HSP-4 homologue GRP78/BiP[32, 34]. The robust translation attenuation observed in ICD-1 depleted embryos under stress is putatively accompanied by an increase in ATF-4, which, in turn, may upregulate HSP-4. Consistently, the recovery of protein synthesis under stress in ICD-2 depleted embryos is potentially due to faster de-repression of translation,

resulting in decreasing levels of ATF4 and therefore HSP-4. To confirm these predictions, ATF-4 levels must be monitored in *C. elegans* embryos depleted of either ICD-1 or ICD-2 with an active UPR.

Although differences in expression of ER specific chaperone and attenuation of protein synthesis under stress were observed in ICD-1 depleted embryos compared to ICD-2 defective embryos (Figure 3 and Figure 11, respectively), depletion of either NAC subunit resulted in equal levels of lysosomal presence (Figure 5). Lysosomal auto fluorescent and HSP-4::GFP images were both analyzed via the fluorescence each element generated. However, whole embryo Z-stacks were generated for HSP-4::GFP samples and single plane images were generated to monitor differences in lysosomal presence. Unlike exogenous fluorophores that are excited at a specific wavelength (as would be true during analysis of HSP-4::GFP), the lysosomal granules were excited with an external fluorescent light and images were captured using a blue filter, which allows light of various wavelengths to be captured. Although the external light source was maintained constant across all samples, the light source may have failed to induce the appropriate excitation/emission spectrum of the auto fluorescent lysosomal granules. Along with inappropriate excitation/emission, the filter employed may not have exclusively captured the desired lysosomal structures. Therefore a more sensitive technique for detection of lysosomal generation may detect differences in lysosomal presence between ICD-1 and ICD-2 depleted embryos.

4.2 tunicamycin exposure leads to differences in neuronal development but not gut cell development between ICD-1 and ICD-2 depleted embryos

In addition to regulating protein homeostasis under stress, both α-NAC and components of the UPR contribute to the differentiation of specific cell types[68-74]. To test whether the individual subunits of the NAC vary in their contributions to differentiation in conjunction with the UPR, the development of neuronal and gut cells was monitored in *C. elegans* strains containing cell-type specific fluorescent reporters.

In early-stage embryos, all RNAi treatments resulted in decreased neuronal YFP signal during sustained tunicamycin exposure compared to untreated samples. However, ICD-1 depleted early embryos showed a significant decrease in YFP signal compared to ICD-2 defective early embryos at 24 hours of tunicamycin exposure (Figure 12). Comparable results were obtained in late-stage embryos: relative to untreated samples, all RNAi treatments resulted in decreased neuronal YFP signal during sustained ER stress with ICD-1 depleted samples showing a significant decrease compared to ICD-2 depleted embryos at 12 hour tunicamycin exposure (Figure 14). During the significant YFP signal reduction observed in ICD-1 depleted embryos, the diffuse YFP signal observed in other treatments became punctate and localized to specific regions of early (Figure 13) and late embryos (Figure 15). The difference in quantified neuronal YFP signal and localization between ICD-1 and ICD-2 depleted embryos occurred during the same tunicamycin exposure times that resulted in significant HSP-4 level differences between the two RNAi treatments. At 12 hour tunicamycin exposure, average YFP pixel intensity in ICD-1 depleted late embryos was 1.5 times lower than ICD-2 defective embryos (Figure 14) and average HSP-4::GFP pixel intensity in ICD-1 depleted embryos was 4 times greater than ICD-2 defective embryos (Figure 3). At 24 hour tunicamycin exposure, average YFP pixel intensity in ICD-1 depleted early embryos was 1.5 times lower than ICD-2

defective embryos (Figure 12) and average HSP-4::GFP pixel intensity in ICD-1 depleted embryos was 3.5 times greater than ICD-2 defective embryos (Figure 3). These observations suggest that disruption of the NAC by depletion of ICD-1 leaves unbound ICD-2 to contribute to the up regulation of HSP-4, which in turn, may alter the normal developmental expression pattern of the specific neuronal marker employed.

The mammalian ICD-2 homologue α-NAC contributes to normal erythroid, CD8+ T cell and osteoblast development; alterations to α-NAC, while β-NAC remains unchanged, leads to altered differentiation in these cell types[68, 69, 70]. Therefore the altered neuronal development observed in our experiments is likely a result of increased levels of unbound ICD-2 in the ICD-1 depleted samples as ICD-2 depleted samples and controls showed virtually equal neuronal differentiation timing. A concomitant increase in HSP-4::GFP was observed during identical tunicamycin exposure times rendering differences in neuronal development between ICD-1 and ICD-2 depleted samples, suggesting an overactive UPR may be sufficient to alter normal cellular development. Like α-NAC, several markers of an active UPR are present during erythroid, CD8+ T cell and osteoblast differentiation[71-74]. Taken together, the results obtained suggest alterations to the normal developmental expression pattern of neurons in *C. elegans* is a result of greater levels of ICD-2 relative to ICD-1 accompanied by an overactive UPR.

Results from FRAP experiments for the specific neuronal marker employed showed ICD-1 depletion led to a stronger suppression of protein synthesis during tunicamycin -induced stress compared to ICD-2 depletion (Figure 11). An identical nematode strain was employed to monitor neuronal development under ER stress in all RNAi treatments. Therefore, the decreased neuronal signal in ICD-1 depleted embryos

observed at 12 (late embryos) and 24 (early embryos) hours tunicamycin exposure may be a reflection of the suppressed translation of the specific neuronal marker employed. If true, a decrease in translation of cell specific markers may be considered inappropriately as a deviation in differentiation. Throughout differentiation, embryos express cell specific markers and a reduction in these markers may be an indication of a subset of cells failing to do so, and attaining an altered cellular "identity". The developmental expression marker under ER stress of a single neuronal marker was monitored in this study. To confirm the observations obtained, other global neuronal and neuron-type specific markers must be similarly assessed.

Although tunicamycin exposure led to a significant reduction in neuronal marker expression in ICD-1 depleted late-stage and early-stage embryos compared to ICD-2 depleted embryos (Figure 12 and Figure 14, respectively), no differences in gut cell expression were found in early-stage or late-stage embryos with identical tunicamycin exposure in either RNAi population (Figure 16 and Figure 17, respectively). This equivalent gut cell development under stress paralleled a significant difference in HSP-4::GFP levels between ICD-1 or ICD-2 depletion (Figure 3). In contrast to the developmental expression of the neuronal marker employed under stress, these observations suggest that the difference in the degree of this UPR induction marker was not sufficient to alter the developmental expression of the gut cell marker employed. However, a single gut cell lineage marker was assessed. To confirm the results obtained, identical experiments should be performed employing a wide range of global gut cell markers.

4.3 Potential role of the *C. elegans* NAC during ER stress and implication for human pathologies

Based on the hypothesized NAC function, disruption of a functional NAC complex may induce the UPR due to inappropriate shuttling of proteins into the ER lumen. Although previous studies have shown removal of either α- or β-NAC can activate the UPR, the degree of UPR induction obtained with removal of one or the other NAC subunit remains unexplored[62, 63]. The individual subunits of the NAC are predicted to possess independent functions that are carried out when unbound from the functional complex, suggesting the hypothesis that disruption of the NAC complex by removal of either subunit leads to unbound levels of an individual subunit that is able to carry out a distinct function[57, 58]. Based on this hypothesis, this study predicted to find differences in major UPR outcomes and development in samples depleted of either α- or β-NAC with an active UPR. Compared to controls, significant differences were found in ICD-1 depleted embryos (β-NAC) presumably containing increased levels of unbound ICD-2 (α -NAC) with an active UPR. These embryos displayed increased HSP-4::GFP levels, a robust suppression of protein synthesis and altered neuronal development relative to ICD-2 (α -NAC) depleted samples. These results are consistent with a NAC subunit specific degree of UPR induction during ER stress and suggest a specific characteristic of the ICD-2 subunit (α -NAC) is responsible for the differences observed in our model system. The role of α-NAC in mammalian bone development provides insights into the results obtained in this study.

Northern blot analysis of developing osteoblast show α-NAC mRNA is higher than that of β-NAC during normal bone development. In this cell type, α-NAC

phosphorylation leads to nuclear translocation where α-NAC acts as a developmentally regulated transcriptional co-activator for ATF4 mediated transcription[70, 71]. As a potent transcription factor during ER stress, ATF4 regulates the expression of ERSE target genes[33]. One of the ATF4 target genes is BiP, the mammalian HSP-4 homologue. ATF4 directly binds the GRP78/BiP promoter region to increase gene expression under stress[34]. This observation is consistent with a previously presented model of an ATF4 mediated HSP-4 up regulation in samples with elevated ICD-2 levels (*icd-1* RNAi) and may explain the differences in the degree of UPR induction obtained with removal of either *C. elegans* NAC subunit. To investigate the potential interactions between ICD-2 and the *C. elegans* ATF-4 homologue, a series of sequence alignments was performed to assess the presence of essential functional features in these proteins.

Phosphorylation of serine 43 in the α-NAC is essential for nuclear translocation to function as a transcriptional co-activator for ATF4 mediated transcription[70, 71]. A protein sequence alignment (Clustal W) between ICD-2 and mammalian α-NAC reveals ICD-2 possesses several conserved serine residues (Figure 18). The functional mammalian ATF4 possesses a conserved Leucine zipper domain composed of repeating Leucine residues near the C′ terminus. In addition, ATF4 is up regulated under stress to induce the expression of ERSE target genes such as the ER specific chaperone GRP78/BiP. ATF5, the *C. elegans* homologue of ATF4, is also up regulated under ER stress to presumably carry out a similar transcriptional induction of ERSE target genes[85]. The sequence alignment performed suggests ICD-2 has the potential for nuclear translocation. In the nucleus, ICD-2 may interact with ATF5 in a complex analogous to that observed during mammalian bone development between α-NAC and ATF4. The predicted

interaction between ICD-2 and ATF5, with elevated levels of ATF5 and greater levels of ICD-2 relative to ICD-1, may target ERSE genes including HSP-4 during ER stress. To test this hypothesis, the outcomes assessed in this study should be tested in embryos depleted of ICD-1 or ICD-2 with an active UPR and containing an ATF5 mutant background. In such future study, the ATF5 mutant background is expected to equilibrate the degree of UPR induction with removal of either subunit based on the resulting outcomes from α-NAC/ATF4 interactions. Consistent with the data presented in this study, the following model suggests a mechanism explaining the differences in the degree of UPR induction obtained with greater levels of ICD-2 relative to ICD-1 (ICD-1 RNAi): (1) tunicamycin activates the UPR, (2) UPR translation attenuation leads to preferential ATF5 translation and (3) ICD-2 phosphorylation leads to nuclear localization and interactions with ATF5 resulting in increased HSP-4 expression, efficient translation attenuation and altered differentiation (Figure 19).

Misfolded protein stress responses are major contributors to the "tipping point" between cell survival and death[1-4]. Based on the functions of α-NAC and the UPR in mitigating stress, it may not be surprising that α-NAC and UPR components are up regulated in certain types of cancers[34, 66, 67]. Using *C. elegans* as a model system, this study found disruption of a functional NAC complex rendering increased unbound α-NAC levels lead to a robust protective response under ER stress. Alterations to α-NAC levels is unlikely the only contributor of a potent UPR under stress. However, a better understanding of the role these factors play on determining the "tipping point" between cell survival and death may help elucidate novel therapeutic targets for diseases exhibiting hyperactive UPR. The increased GRP78/BiP expression documented in tumor

cells is likely representative of a hyperactive protective response under ER stress and reflects a "tipping point" predisposed towards survival. Based on previous studies and the data presented in this study, NAC may serve as a target for reconstituting the appropriate "tipping point" in cells predisposed towards survival[66, 67]. Given the complexity of the different components of the UPR, it is likely that α-NAC interacts differently with each arm of the UPR. *C.elegans* provide an appropriate system to explore the direction in which the "tipping point" is predisposed in samples defective of certain UPR components. A lucid understanding of the mechanism by which interactions between α-NAC and individual UPR components affect cell fate will provide further potential therapeutic targets for diseases exhibiting alterations in UPR activity, such as neurodegeneration and cancer.

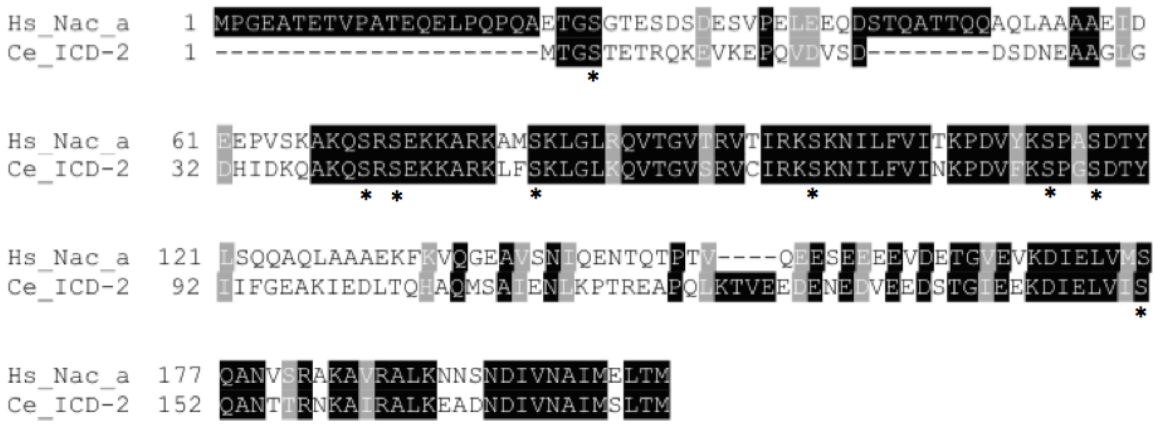

Figure 18: **Protein sequence alignment of mammalian α-NAC and *C. elegans* icd-2.** A protein sequence alignment (Clustal W) was performed to compare the amino acid sequence composition of mammalian α-NAC (Hs_Nac_a) and *C. elegans* ICD-2 (Ce_ICD-2). Asterisks denote conserved serine residues amongst the two protein sequences

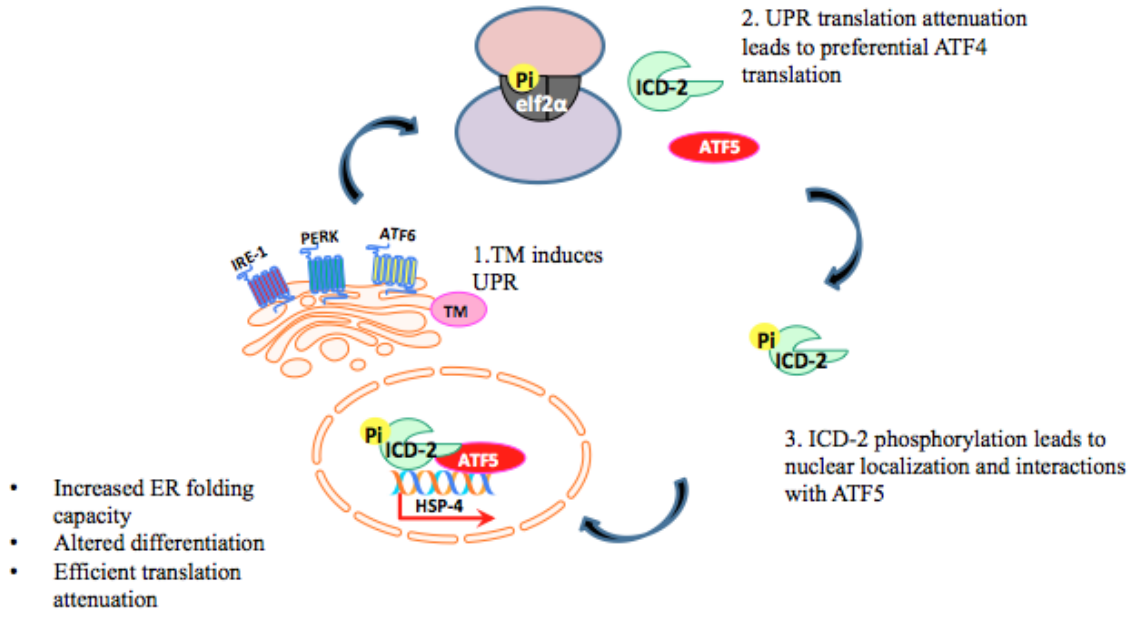

Figure 19: **Proposed mechanism for differences in the degree of UPR induction obtained with elevated ICD-2 levels.** (1) Tunicamycin activates the UPR, (2) UPR translation attenuation leads to preferential ATF-5 translation and (3) ICD-2 phosphorylation leads to nuclear localization and interactions with ATF-5 resulting in increased HSP-4 expression, efficient translation attenuation and altered differentiation

References

1. Dobson, C.M., Hore, P.J. (1998) Kinetic studies of protein folding using NMR spectroscopy. *Nature struct. Biol.,* 5:504-507.
2. Dobson, C.M., Karplus, M. (1999) The fundamentals of protein folding: bringing together theory and experiment. *Curr. Opin. Struct. Biol.,* 9:92-101.
3. Dyson, H.J., Wright, P.E. (1998) Equilibrium NMR studies of unfolded and partially folded proteins. *Nature Struct. Biol.,* 5:499-503.
4. Bryngelson, J.D., Onuchic, J.N., Socci, N.D., Wolynes, P.G. (1995) Funnels, pathways and the energy landscape of protein folding: a synthesis. *Proteins,* 21:167-195.
5. Dobson, C.M. (2001) The structural basis of protein folding and its links with human disease. *Phil. Trans. R. Soc. Lond. B*., 356:133-145.
6. Gething, M.J., Sambrook, J. (1992) Protein folding in the cell. *Nature,* 355:33-45.
7. Ellis, R.J., Hartl, F.U. (1999) Principles of protein folding in the cellular environment. *Curr. Opin. Struct. Biol.,* 9:101-110.
8. Anfinsen, C.B. (1973) Principles that govern the folding of protein chains. *Science,* 181:223-230
9. Lee, C., Yu, M. (2005) protein folding and disease. *Journal of biochemistry and molecular biology,* 38:275-280.
10. Fink, S.L., Cookson, B.T. (2005) Apoptosis, Pyroptosis, and Necrosis: Mechanistic Description of Dead and Dying Eukaryotic Cells. *Infect. Imm*., 73:1907-1916.

11. Ross, C.A., Poirier, M.A. (2004) Protein aggregation and neurodegenerative disease. *Nature medicine,* 10:10-17.

12. Whitesell, L., Lindquist, S. (2005) HSP90 and the chaperoning of cancer. *Nat. rev. cancer,* 10:761-772.

13. Agorogiannis, E.I., Agorogiannis, G.I., Papadimitriou, G.M., Hadjigeorgiou, G.M. (2004) Protein misfolding in neurodegenerative disease. *Neuropathology and applied neurobiology,* 30:215-224.

14. Steffani, M., Dobson, C.M. (2003) Protein aggregation and aggregate toxicity: new insights into protein folding, misfolding diseases and biological evolution. *Journal of molecular medicine,* 81:678-699.

15. Hartl, F.U., Hayer-Hartl, M. (2002) Molecular chaperones in the cytosol: from nascent chain to folded protein. *Science,* 295:1852-1858.

16. Hardesty, B., Kramer, G. (2001) Folding of a nascent peptide on the ribosome. *Prog. Nucleic Acid Res. Mol. Biol.,* 66:41-66.

17. Thomas, P.J., Qu, B.H., Pederson, P.L. (1995) Defective protein folding as the basis of human disease. *Trends Biochem. Sci.,* 20:456-459.

18. Yoo, C. B., Kim, S. H., Cairns, N., Fountoulakis, M., Lubec, G. (2001) Deranged expression of molecular chaperones in brains of patients with Alzheimer's disease. *Biochemical and Biophysical research communications,* 280:249-258.

19. Yamaguchi, Y., Larkin, D., Lara-Lemus, R., Ramos-Castañeda, J., Liu, M., Arvan, P. (2008) Endoplasmic Reticulum (ER) Chaperone Regulation and Survival of Cells Compensating for Deficiency in the ER Stress Response Kinase, PERK. *Journal of biological chemistry*, 283:17020-17029.

20. Li, X., Zhang, K., Li, Z. (2011) Unfolded protein response in cancer: the physicians perspective. *Journal of hematology and oncology,* 4:1-10.

21. Greavs, M., Maley, C.C. (2012) Clonal evolution in cancer. *Nature* 481:306-313.

22. Oren, M. (1999) Regulation of the p53 tumor suppressor protein. *Journal of biological chemistry,* 51:36031-36034.

23. Van Drie, J.H. (2011) Protein folding, protein homeostasis, and cancer. *Chinese journal of cancer,* 30:124-137.

24. Sitia, R., Braakman, I. (2003) Quality control in the endoplasmic reticulum protein factory. *Nature,* 426:891-894.

25. Welch, W.J. (2004) Role of quality control pathways in human disease involving protein misfolding. *Semin. Cell Dev. Biol.,* 15:31-38.

26. Meunier, L., Usherwood, Y.K., Chung, K.T., Hendershot, L.M. (2002) A subset of chaperones and folding enzymes form multiprotein complexes in endoplastic reticulum to bind nascent proteins. *Mol Biol. Cell*, 13:4456-4469.

27. Schroder, M., Kaufman, R.J. (2005) ER stress and the unfolded protein response. *Mutat. Res.,* 569:29-63.

28. Lee AS. The ER chaperone and signaling regulator GRP78/BiP as a monitor of endoplasmic reticulum stress. *Methods*, 2005(35):373–381.

29. Kawaguchi, S. and Ng, D.T. (2011). Cell biology. Sensing ER stress. *Science,* 333(6051):1830–1831.

30. Harding, H.P., Zhang, Y., Ron, D., (1999) Protein translation and folding are coupled by an endoplasmic-reticulum-resident kinase. *Nature*, (397):271–274.

31. Shi, Y., Vattem, K.M., Sood, R., An, J., Liang, J., Stramm, L., Wek, R.C. (1998) Identification and characterization of pancreatic eukaryotic initiation factor 2 alpha-subunit kinase, PEK, involved in translational control. *Mol Cell Biol.*, (18):7499–7509.

32. Marciniak, S.J., Yun., C.Y., Oyadomari, S., Novoa, I., Zhang, Y., Jungreis, R., Nagata, K., Harding, H.P., Ron, D., (2004) CHOP induces death by promoting protein synthesis and oxidation in the stressed endoplasmic reticulum. *Genes Dev.*, 18(24):3066-77.

33. Luo, S., Baumeister, P., Yang, S., Abcouwer, S.F., Lee, A.S. (2003) Induction of GRP78/BiP by translational block: activation of the GRP78 promoter by ATF4 through and upstream ATF/CRE site independent of the endoplasmic reticulum stress elements. *J Biol Chem.*, 278(39):37375-85.

34. Chang, S.C., Erwin, A.E., Lee, A.S. (1989) Glucose-regulated protein (GRP94 and GRP78) genes share common regulatory domains and are coordinately regulated by common trans-acting factors. *Mol. Cell. Biol.***,** 9(5):2153-2162.

35. Haze, K., Yoshida, H., Yanagi, H., Yura, T., Mori, K., (1999) Mammalian transcription factor ATF6 is synthesized as a transmembrane protein and activated by proteolysis in response to endoplasmic reticulum stress. *Mol Biol Cell.,* 10:3787–3799.

36. Li, M., Baumeister, P., Roy, B., Phan, T., Foti, D., Luo, S., Lee, A.S. (2000) ATF6 as a transcription activator of the endoplasmic reticulum stress element: thapsigargin stress-induced changes and synergistic interactions with NF-Y and YY1. *Mol Cell Biol*., 20:5096–5106.

37. Calfon, M., Huiqing, Z., Fumihiko, U., Till, J. H., Hubbard, S. R., Harding, H. P., Clark, S.G. and Ron, D. (2002) IRE1 couples endoplasmic reticulum load to secretory capacity by processing the XBP-1 mRNA. *Nature* 415(6867):92-96.

38. Lehman, N.L. (2009) The ubiquitin proteasome system in neuropathology. *Acta Neuropathologica,* 118(3):329–347.

39. Cherra, S.J., Dagda, R.K., Chu, C.T. (2010) Review: autophagy and neurodegeneration: survival at a cost? *Neuropathology and applied neurobiology,* 36(2):125–132.

40. Tanida, I., Ueno, T., Kominami, E. (2004) LC3 conjugation system in mammalian autophagy. *The international journal of biochemistry and cell biology,* 36(12):2503–2518.

41. Kouroku, Y., Fujita, E., Tanida, I., Ueno, T., Isoai, A., Kumagai, H., Ogawa, S., Kaufman, R.J., Kominami, E., Momoi, T. (2007) ER stress (PERK/eIF2a phosphorylation) mediates the polyglutamine induced LC3 conversion, an essential step for autophagy formation. *Cell Death Differ*, 14:230-239

42. Rao, R.V., Castro-Obregon, S., Frankowski, H., Schuler, M., Stroka, V., Del Rio, G., Bredesen, D.E., Ellerby, H.M. (2002) Coupling endoplasmic reticulum stress to the cell death program. An Apaf-1 independent intrinsic pathway. *J. Biol. Chem.,* 277:21836-21842.

43. Wiedmann, B., Sakai, H., Davis, T.A., Wiedmann, M. (1994) A protein complex required for signal-sequence specific sorting and translocation. *Nature*, 370:434-440.

44. Wegrzyn, R. D., Diana, H., Frieder, M., Rainer, N., Rauch, T., Graf, C. and Elke, D. (2006) A conserved motif is prerequisite for the interaction of NAC with ribosomal protein L23 and nascent chains. *Journal of Biological Chemistry* 281(5):2847-2857.

45. Kanki,T.,Wang,K.,andKlionsky,D.J.(2010).Agenomic screenforyeastmutantsdefectiveinmitophagy.Autophagy,6(2):278–280

46. Rospert, S., Dubaqui, Y., and Gautschi, M. (2002) Nascent-polypeptide-associated complex. *Cellular and Molecular Life Sciences,* 59(10):1632–1639.

47. Koplin, A., Preissler, S., Ilina, Y., Koch, M., Scior, A., Erhardt, M., and Deuerling, E.(2010) A dual function for chaperone sssb-rac and the nac nascent polypeptide-associated complex on ribosomes. *The Journal of cell biology,* 189(1):57–68.

48. Karbstein, K. (2010) Chaperoning ribosome assembly. *The Journal of cell biology,* 189(1):11–12.

49. Del Alamo, M., Hogan, D.J., Pechmann, S., Albanese, V., Brown, P.O., and Frydman, J. (2011) Defining the specificity of cotranslationally acting chaperones by systematic analysis of mRNAs associated with ribosome nascent chain complexes. *PLoS biology,* 9(7):e1001100

50. Wegrzyn, R.D., Hofmann, D., Merz, F., Nikolay, R., Rauch, T., Graf, C., and Deuerling, E. (2006) A conserved motifis prerequisite for the interaction of NAC with ribosomal protein l23 and nascent chains. *The Journal of biological chemistry,* 281(5):2847–2857.

51. Pech, M., Spreter, T., Beckmann, R., and Beatrix, B. (2010) Dual binding mode of the nascent polypeptide-associated complex reveals a novel universal adapter site on the ribosome. *The Journal of biological chemistry,* 285(25):19679–19687.

52. Beatrix, B., Sakai, H., and Wiedmann, M. (2000) The alpha and beta subunit of the nascent polypeptide-associated complex have distinct functions. *The Journal of biological chemistry,* 275(4):37838–37845.

53. Liu, Y., Hu, Y., Li, X., Niu, L., and Teng, M. (2010) The crystal structure of the human nascent polypeptide-associated complex domain reveals a nucleic acid-binding region on the NACA subunit. *Biochemistry,* 49(13):2890–2896.

54. Peisker, K., Braun, D., Wolfle, T., Hentschel, J., Funfschilling, U., Fischer, G., Sickmann, A., and Rospert, S. (2008) Ribosome-associated complex binds to ribosomes in close proximity of rpl31 at the exit of the polypeptide tunnel in yeast. *Molecular biology of the cell,* 19(12):5279–5288.

55. Halic, M., Gartmann, M., Schlenker, O., Mielke, T., Pool, M. R., Sinning, I., and Beckmann, R. (2006) Signal recognition particle receptor exposes the ribosomal translocon binding site. *Science,* 312(5774):745-747.

56. Liu, Y., Hu, Y., Li, X., Niu, L., and Teng, M. (2010) The crystal structure of the human nascent polypeptide-associated complex domain reveals a nucleic acid-binding region on the NACA subunit. *Biochemistry,* 49(13):2890-2896.

57. Kristein-Miles, J., Scior, A., Deuerling, E., Morimoto, R. (2013) The nascent polypeptide-associated complex is a key regulator of proteostasis. *The EMBO journal*, 10:1461-1468.

58. Moreau, A., Yotov, W. V., Glorieux, F. H., and St-Arnaud, R. (1998) Bone-specific expression of the alpha chain of the nascent polypeptide-associated complex, a coactivator potentiating c-Jun-mediated transcription. *Molecular and cellular biology,* 18(3):1312-1321.

59. Reimann, B., Bradsher, J., Franke, J., Hartmann, E., Wiedmann, M., Prehn, S., and Wiedmann, B .(1999) Initial characterization of the nascent polypeptide-associated complex in yeast. *Yeast*, 15:397–407.

60. Markesic, D.C., Gajewski, K.M., Nazimiec, M.E., Beckingham, K. (2000) Bicaudal encodes the *Drosophila* beta NAC homolog, a component of the ribosomal translational machinery. *Development*, 127:559–572.

61. Den, J.M., Behringer, R.R. (1995) An insertion in the BTF3 transcription factor gene leads to an early postimplantation lethality in mice. *Transgenic Res*, 4:264–269.

62. Arsenovic, P.T., Maldonado, A.T., Colleluori, V.D., Bloss, T.A. (2012) Depletion of the C. elegans NAC engages the unfolded protein response, resulting in increased chaperone expression and apoptosis. *Plos one,* 7:1-12.

63. Hotokezaka, Y., van Leyen, K., Lo, E. H., Beatrix, B., Katayama, I., Jin, G., and Nakamura, T. (2009) αNAC depletion as an initiator of ER stress-induced apoptosis in hypoxia. *Cell Death & Differentiation,* 16(11):1505-1514.

64. Bloss, T.A., Witze, E.S., Rothman, J.H. (2003) Supression of CED-3 independent apoptosis by mitochondrial βNAC in C. elegans. *Letters to nature,* 424:1066-1071

65. Zeng, W., Zhang, J., Qi, M., Peng, C., Su, J., Chen, X., and Yuan, Z. (2014) αNAC inhibition of the FADD-JNK axis plays anti-apoptotic role in multiple cancer cells. *Cell Death & Disease,* 5(6)e1282.

66. Kim, S.H., Shim, K.S., Lubec, G., (2002) Human brain nascent polypeptide-associated complex a subunit is decreased in patients with Alzheimer's disease and Down syndrome. *J Investing Med,* 50: 293–301.

67. Kroes, R.A., Jastrow, A., McLone, M.G., Yamamoto, H., Colley, P., Kersey, D.S., Moskal, J.R. (2000) The identification of novel therapeutic targets for the treatment of malignant brain tumors. *Cancer Lett,* 156:191–198.

68. Lopez, S., Stuhl, L., Fichelson, S., Dubart-Kupperschmitt, A., St Arnaud, R., Galindo, J. R., and Gomez, S. (2005) NACA is a positive regulator of human erythroid-cell differentiation. *Journal of cell science,* 118(8):1595-1605.

69. Al-Shanti, N., and Ziyad, A. (2006) Inhibition of alpha nascent polypeptide associated complex protein may induce proliferation, differentiation and enhance the cytotoxic activity of human CD8+ T cells. *Journal of clinical immunology,* 26(5):457-464.

70. Meury, T., Akhouayri, O., Jafarov, T., and St-Arnaud, R. (2010) Nuclear αNAC influences bone matrix mineralization and osteoblast maturation in vivo. *Molecular and cellular biology,* 30(1):43-53.

71. St-Arnaud, R., and Bahareh, H. (2011) Combinatorial control of ATF4-dependent gene transcription in osteoblasts. *Annals of the New York Academy of Sciences,* 1237(1):11-18.

72. van Galen, P., Kreso, A., Mbong, N., Kent, D. G., Fitzmaurice, T., Chambers, J. E., and Dick, J. E. (2014) The unfolded protein response governs integrity of the haematopoietic stem-cell pool during stress. *Nature,*

73. Brunsing, R., Omori, S. A., Weber, F., Bicknell, A., Friend, L., Rickert, R., and Niwa, M. (2008) B-and T-cell development both involve activity of the unfolded protein response pathway. *Journal of Biological Chemistry,* 283(26):17954-17961.

74. Tohmonda, T., Miyauchi, Y., Ghosh, R., Yoda, M., Uchikawa, S., Takito, J., and Horiuchi, K. (2011) The IRE1α−XBP1 pathway is essential for osteoblast differentiation through promoting transcription of Osterix. *EMBO reports,* 12(5):451-457.

75. Lettre, G., Hengartner, M.O. (2006) Developmental apoptosis in C. elegans: a complex CEDnario. *Developmental cell biology* 7:91-108.

76. Noda, I., Fujieda, S., Seki, M., Tanaka, N., Sunaga, H., Ohtsubo, T., Tsuzuki, H., Fan, G. K., and Saito, H. (1999) Inhibition of n-linked glycosylation by tunicamycin enhances sensitivity to cisplatin in human head-and-neck carcinoma cells. *International journal of cancer,* 80(2):279−284.

77. Calfon, M., Zeng, H., Urano, F., Till, J. H., Hubbard, S. R., Harding, H. P., Clark, S. G., and Ron, D. (2002) IRE-1 couples endoplasmic reticulum load to secretory capacity by processing the xbp-1 mrna. *Nature,* 415(6867):92− 96.

78. røkjær-Jensen, C., Davis, M. W., Sarov, M., Taylor, J., Flibotte, S., LaBella, M., and Jorgensen, E. M. (2014) Random and targeted transgene insertion in

Caenorhabditis elegans using a modified Mos1 transposon. *Nature methods,* 11(5):529-534.

79. Lu, N., Yu, X., He, X., and Zhou, Z. (2009) Detecting apoptotic cells and monitoring their clearance in the nematode Caenorhabditis elegans. *Apoptosis*, 357-370.
80. Kourtis, N., and Nektarios, T. (2009) Cell-specific monitoring of protein synthesis in vivo. *PloS one,* 4(2):e4547.
81. Coburn, C., and Gems, D. (2013) The mysterious case of the C. elegans gut granule: death fluorescence, anthranilic acid and the kynurenine pathway. *Frontiers in genetics* 4.
82. Calfon, M., Huiqing Z., Fumihiko., Till, J. H., Hubbard, S. R., Harding, H. P., Clark, S. G., and Ron, D. (2002) IRE1 couples endoplasmic reticulum load to secretory capacity by processing the XBP-1 mRNA. *Nature* (415) 6867:92-96.
83. Calixto, A., Dattananda C., Irini, T., Xiaoyin C., and Martin C. (2010) Enhanced neuronal RNAi in C. elegans using SID-1. *Nature methods* (7) 7:554-559.
84. Zhang, S. O., Andrew C. B., Ningyi, X., Johan L. M., Jingyi, Y., Fengli, G., Rhonda, T., and Ho, Y. M. (2010) Genetic and dietary regulation of lipid droplet expansion in Caenorhabditis elegans. *Proceedings of the National Academy of Sciences* (107) 10:4640-4645.
85. Zhou, D., Reddy, L., Palam, Jiang, L., Narasimhan, J., Staschke, K. A. and Wek, R. C. (2008) Phosphorylation of eIF2 directs ATF5 translational control in response to diverse stress conditions. *Journal of Biological Chemistry* (283) 11:7064-7073.